The FeoC [4Fe-4S] cluster is redox-active and rapidly oxygen-sensitive

Aaron T. Smith[1*], Richard O. Linkous[1], Nathan J. Max[1], Alexandrea E. Sestok[1], Veronika A. Szalai[2], and Kelly N. Chacón[3]

[1]Department of Chemistry and Biochemistry, University of Maryland, Baltimore County, Baltimore, Maryland, 21250 USA

[2]Physical Measurement Laboratory, National Institute of Standards and Technology, Gaithersburg, Maryland, 20899, USA

[3]Department of Chemistry, Reed College, Portland, Oregon, 97202, USA

[*]To whom correspondence should be addressed. Tel: 410-455-1985; E-mail: smitha@umbc.edu

Abstract

The acquisition of iron is essential to establishing virulence among most pathogens. Under acidic and/or anaerobic conditions, most bacteria utilize the widely-distributed ferrous iron (Fe^{2+}) uptake (Feo) system to import metabolically-required iron. The Feo system is inadequately understood at the atomic, molecular, and mechanistic levels, but we do know it is composed of a main membrane component (FeoB) essential for iron translocation, as well as two small, cytosolic proteins (FeoA and FeoC) hypothesized to function as accessories to this process. FeoC has many hypothetical functions, including that of an iron-responsive transcriptional regulator. Here, we demonstrate for the first time that *Escherichia coli* FeoC (*Ec*FeoC) binds an [Fe-S] cluster. Using electronic absorption, X-ray absorption, and electron paramagnetic resonance spectroscopies, we extensively characterize the nature of this cluster. Under strictly anaerobic conditions after chemical reconstitution, we demonstrate that *Ec*FeoC binds a redox-active $[4Fe\text{-}4S]^{2+/+}$ cluster that is rapidly oxygen-sensitive and decays to a $[2Fe\text{-}2S]^{2+}$ cluster ($t_{½} \approx 20$ s), similar to the [Fe-S] cluster in the fumarate and nitrate reductase (FNR) transcriptional regulator. We further show that this behavior is nearly identical to the homologous *K. pneumoniae* FeoC, suggesting a redox-active, oxygen-sensitive $[4Fe\text{-}4S]^{2+}$ cofactor is a general phenomenon of cluster-binding FeoCs. Finally, in contrast to FNR, we show that $[4Fe\text{-}4S]^{2+}$ cluster binding to FeoC is associated with modest conformational changes of the polypeptide, but not protein dimerization. We thus posit a working hypothesis in which the cluster-binding FeoCs may function as oxygen-sensitive iron sensors that fine-tune pathogenic ferrous iron acquisition.

Abbreviations

CD, circular dichroism; DLS, dynamic light scattering; DTT, dithiothreitol; EDTA, ethylenediaminetetraacetic acid; EPR, electron paramagnetic resonance; EXAFS, extended X-ray absorption fine structure; FNR, fumarate and nitrate reductase; FUR, ferric uptake regulator; GDP, guanosine diphosphate; GTP, guanosine triphosphate; HiPIP, high potential iron-sulfur protein; HTH, helix-turn-helix; MBP, maltose-binding protein; MOPS, 3-(*N*-morpholino)propanesulfonic acid; NFeoB, soluble N-terminal GTP-binding domain of FeoB; SDS-PAGE, sodium dodecyl sulfate polyacrylamide gel electrophoresis; SEC, size-exclusion chromatography; TEV, Tobacco Etch Virus; Tris, tris(hydroxymethyl)aminomethane; TCEP, tris(2-carboxyethyl)phosphine; XAS, X-ray absorption spectroscopy.

Introduction

Iron is an essential element in numerous indispensable biological processes thus necessitating its availability for the survival of virtually every organism.[1-3] For disease-causing bacteria, the acquisition of iron is an essential virulence factor for the establishment of infection.[4-6] During this process, the host is typically the source of bacterial iron, where it may be found in multiple oxidation and/or coordination states, necessitating pathogens to adapt to acquire iron in ferric (Fe^{3+}), ferrous (Fe^{2+}), and even chelated forms.[5-7] Because each oxidation state of iron may have different ligand preferences, metal-ligand distances, and even metal ion lability, bacteria must maintain multiple transport systems to handle these various forms of this vital element. Under oxidizing conditions, siderophore- and/or heme-based acquisition systems are commonly used by many bacteria to stabilize, to solubilize, and to transport ferric iron. Under acidic, micro-aerobic, and/or anaerobic conditions, such as those found in the gut or within biofilms, iron may be prevalent and soluble in the reduced, ferrous form.[7]

The ferrous iron transport system, also known as Feo, is the predominant prokaryotic Fe^{2+} transport pathway. This system is encoded by the *feo* operon (Fig. 1A), which was first discovered in *Escherichia coli* K-12.[7-9] In many bacteria, upstream of the *feo* operon are binding sites for two transcriptional regulators: the ferric uptake regulator (FUR), a global iron regulator controlling transcription of numerous genes involved in iron utilization and metabolism; and the fumarate and nitrate reductase (FNR) regulator, a global iron-based regulator controlling transcription of genes involved in processes linked to anaerobic metabolism.[9, 10] Downstream of these transcriptional regulator binding sites in *E. coli* K-12 are encoding regions for three proteins (Fig. 1A): FeoA, a small, cytosolic β-barrel protein thought to be an integral regulatory element; FeoB, a large polytopic membrane protein bearing a N-terminal GTP-binding domain that moves ferrous iron

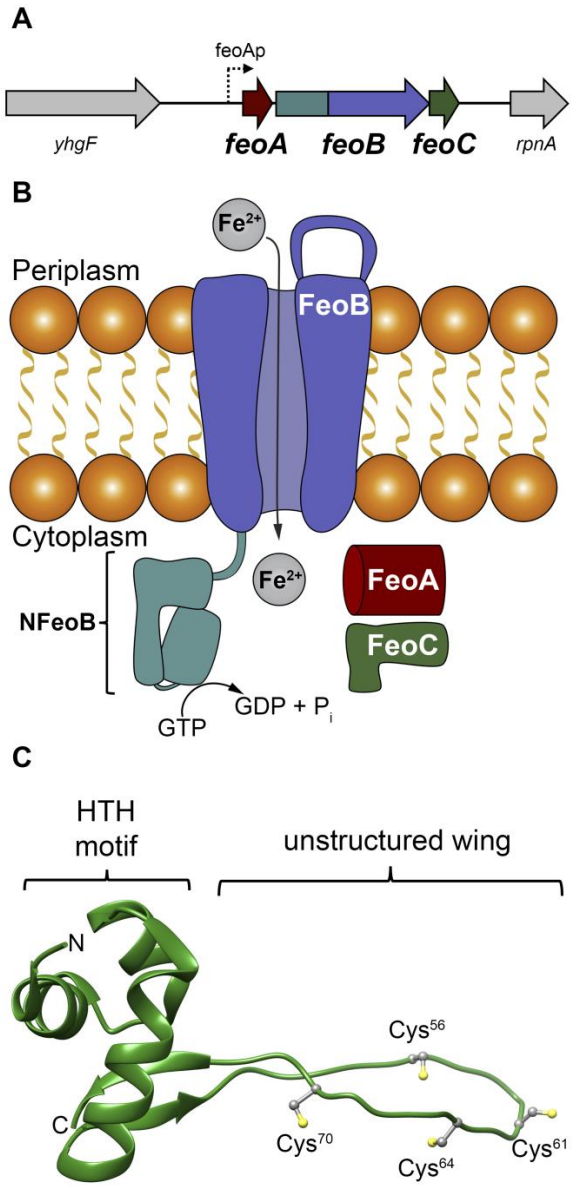

Figure 1. The Feo system and the structure of *E. coli* FeoC. **A**. The arrangement of the *feo* operon in *E. coli* K-12, which encodes for three proteins: FeoA, FeoB, FeoC. FeoAp represents the location of the FeoA promoter. To emphasize the co-transcription of the components of the *feo* operon, the physical layout of neighboring genes such as a putative RNA-binding protein (encoded by *yhgF*) and a downstream nuclease (encoded by *rpnA*) is included. **B**. Cartoon of the Feo system in *E. coli*. FeoA (red) and FeoC (green) are small cytosolic proteins that may function as regulatory accessories to control ferrous (Fe^{2+}) iron transport. Movement of ferrous iron across a cellular membrane is accomplished by the large, polytopic membrane protein FeoB (purple). Hydrolysis of GTP to GDP within the N-terminal soluble GTP-binding domain of FeoB (NFeoB, teal) is thought to regulate opening and closing of FeoB, but it is unknown whether this process is driven in an active or facilitated manner. **C**. Lowest-energy NMR conformer of *Ec*FeoC (PDB ID 1XN7). Labeled regions are: the helix-turn-helix (HTH) motif and the unstructured wing region that contains four Cys residues (Cys^{56}, Cys^{61}, Cys^{64} and Cys^{70}) involved in [Fe-S] cluster binding. The labels "N" and "C" represent the amino and carboxy termini, respectively.

across the membrane; and FeoC, a small, cytosolic winged-helix protein with an unknown function. In a Gram-negative bacterium such as *E. coli* K-12, these three proteins are thought to function in concert to regulate the movement of ferrous iron into the cytosol to be incorporated into the intracellular labile iron pool (Fig. 1B).[7]

Although ferric siderophore- and heme-transport systems have been historically recognized as important contributors to bacterial virulence,[11-13] emerging evidence demonstrates that ferrous iron contributes significantly to the establishment of infection by a wide array of pathogens within mammalian hosts. For example, FeoA and FeoB knockouts in model pathogens have decreased or abrogated growth of several strains.[14-18] Additionally, gene knockouts of the *feo* operon native to several human pathogens have either reduced[19, 20] or wholly prevented[4] colonization of these bacteria within mouse,[4] chicken,[21] and/or piglet models,[21] emphasizing the importance of this uptake pathway to bacterial infection within mammals and birds. Organisms whose normal iron homeostasis appears to be dependent either in part or wholly on the Feo system include several acute, and multiple emergent pathogens, such as *Campylobacter jejuni*,[21] *E. coli*,[22] *Francisella tularensis*,[23] *Helicobacter pylori*,[4] *Porphyromonas gingivalis*,[15, 16] *Shigella flexneri*,[24] *Vibrio cholerae*,[25] and even *Yersinia pestis*,[26] underscoring the importance of ferrous iron uptake to several disease-causing bacteria. A definitive consensus regarding the contribution of Feo towards virulence and growth of the opportunistic pathogen *Pseudomonas aeruginosa* remains somewhat controversial.[27, 28] However, recent findings have indicated substantive concentrations of ferrous iron (≈ 40 μmol/L) within the sputum of patients suffering from cystic fibrosis,[29] and iron availability is strongly linked to *P. aeruginosa* biofilm formation,[30, 31] disease progression, and disease severity.[29] Thus it is clear that Feo-mediated ferrous iron uptake contributes

significantly to bacterial virulence, and a greater structural and mechanistic understanding of this system could allow for the rational targeting of Feo for antibacterial developments.

To this end, we initially sought to biochemically, biophysically, and spectroscopically characterize the FeoC component of unknown function from the Gram-negative bacterium *E. coli* K-12 (*Ec*FeoC). A prior bioinformatics analysis has suggested that FeoCs are found in approximately 15% of all *feo* operons and are common to γ-proteobacteria.[32] NMR structures of intact *E. coli* (Fig. 1C; PDB ID 1XN7) and *Klebsiella pneumoniae* FeoC (*Kp*FeoC; PDB ID 2K02)[33] reveal an overall fold consisting of a LysR-like winged-helix motif, implicating these proteins as potential transcriptional regulators. Within the disordered "wing" of these structures are 4 Cys residues (Fig. 1C) that are strongly conserved[34] and are speculated to bind an [Fe-S] cluster, which could structure this region to drive function. In support of this hypothesis, a study of recombinant *Kp*FeoC demonstrated the presence of an [Fe-S] cluster bound to this protein in low yield under aerobic conditions;[34] however, this previous work assigned the *Kp*FeoC cluster to an unusual $[4Fe\text{-}4S]^{3+}$ high potential iron-sulfur protein (HiPIP)-like state that was exceptionally oxygen-tolerant, leading us to question the validity of this assignment.

In this work, we demonstrate that *Ec*FeoC binds an [Fe-S] cluster, and we spectroscopically and biophysically characterize the nature of this cluster. Under strictly anaerobic conditions, we demonstrate that *Ec*FeoC binds a redox-active and rapidly oxygen-sensitive $[4Fe\text{-}4S]^{2+/+}$ cluster, in distinct contrast to studies of *Kp*FeoC. To rectify this discrepancy, we then spectroscopically and biophysically characterize the nature of the *Kp*FeoC [Fe-S] cluster and find it to behave nearly identically to that of *Ec*FeoC in our hands. We suggest that previous aerobic handling of the oxygen-sensitive *Kp*FeoC may have led to the incorrect cluster assignment. Finally, we show that this cluster binding is associated with modest conformational changes of both *Ec*- and *Kp*FeoC but

not protein dimerization, and we speculate how this cluster binding and conformational change may relate to the function of FeoC.

Materials and Methods

Materials. All materials used for buffer preparation, protein expression, and protein purification were purchased from standard commercial suppliers and were used as received. Where indicated, values are reported as the mean ± one standard deviation. Note that certain commercial equipment, instruments, or materials are identified in this paper to specify the experimental procedure adequately. Such identification is not intended to imply recommendation or endorsement by the National Institute of Standards and Technology, nor is it intended to imply that the materials or equipment identified are necessarily the best available for the purpose.

Cloning, Expression, Purification, and Cleavage of Ec- and KpFeoC. DNA encoding for the genes corresponding to FeoC from *Escherichia coli* (strain K-12) (Uniprot identifier P64638) (*Ec*FeoC) and from *Klebsiella pneumoniae* (strain 342) (Uniprot identifier B5XTS6) (*Kp*FeoC) were commercially synthesized by GenScript (Piscataway, NJ), with additionally engineered DNA sequences encoding for a C-terminal TEV-protease cleavage site (ENLYFQG) or with an additionally engineered DNA sequence encoding for an N-terminal maltose-binding protein sequence (based on P0AEX9: *Escherichia coli* (K-12) *malE* gene product) followed by a Tobacco Etch Virus (TEV)-protease cleavage site. For the former approach, the gene was subcloned into the pET-21a(+) expression plasmid using the NdeI and XhoI restriction sites, encoding for a C-terminal $(His)_6$ affinity tag when read in-frame. For the latter approach, gene was subcloned into the pET-45b(+) expression plasmid using the PmlI and PacI restriction sites, encoding for a N-terminal $(His)_6$ affinity tag followed by maltose-binding protein when read in-frame.

The complete expression plasmid was transformed into chemically competent BL21(DE3) cells, spread onto Luria-Bertani (LB) agar plates supplemented with 100 μg/mL ampicillin (final concentration), and grown overnight at 37 °C. Colonies from these plates served as the source of

E. coli for small-scale starter cultures (generally 100 mL LB supplemented with 100 μg/mL ampicillin as a final concentration). Large-scale expression of each construct was accomplished in 12 baffled flasks each containing 1 L LB supplemented with 100 μg/mL (final concentration) ampicillin and inoculated with a pre-culture. Cells were grown by incubating these flasks at 37 °C with shaking until the optical density at 600 nm (OD_{600}) was approximately 0.6 to 0.8. The flasks containing cells and media were then removed from the incubator shaker and chilled to 4 °C in a cold room. After 2 h at 4 °C, protein expression was induced by the addition of isopropyl β-D-l-thiogalactopyranoside (IPTG) to a final concentration of 1 mmol/L, and the flasks were transferred back to the incubator shaker operating at 18 °C with shaking at 20.9 rad/s (200 rpm). After approximately 18 h to 20 h, cells were harvested by centrifugation at 4800×*g*, 10 min, 4 °C. Cell pellets were subsequently resuspended in resuspension buffer (50 mmol/L Tris, pH 7.5, 200 mmol/L NaCl, 0.7 mol/L glycerol (5 % (v/v)) to a concentration of ≈ 0.4 g cells per mL buffer, flash-frozen on $N_{2(l)}$, and stored at -80 °C until further use.

All steps for the purification of MBP-*Ec*FeoC and MBP-*Kp*FeoC were performed at 4 °C unless otherwise noted. Frozen cells were thawed and stirred at room temperature until the solution was homogeneous. Solid phenylmethylsulfonyl fluoride (PMSF; ≈ 50 mg to 100 mg) was added immediately prior to cellular disruption using a Q700 ultrasonic cell disruptor. Cellular debris was cleared by ultracentrifugation at 163000×*g* for 1 h. The supernatant was then applied to two tandem 5 mL MBPTrap HP columns that had been pre-equilibrated with 5 column volumes (CVs) of wash buffer (25 mmol/L Tris, pH 7.5, 200 mmol/L NaCl, 0.7 mol/L glycerol (5% (v/v)), 1 mmol/L TCEP). The column was then washed with 20 CVs of wash buffer. Protein was then eluted by wash buffer containing 10 mmol/L maltose. Fractions were concentrated using a 15 mL Amicon 30 kg/mol (30 kDa) molecular-weight cutoff (MWCO) spin concentrator. Protein was then buffer

exchanged in the same spin concentrator by repeated dilution and concentration into TEV protease buffer (50 mmol/L Tris, pH 8.0, 200 mmol/L NaCl, 0.7 mol/L glycerol (5% (v/v)), 1 mmol/L TCEP, 0.5 mmol/L EDTA). Cleavage, which liberates native FeoC with an additional Gly residue on its N-terminus, was accomplished by mixing ≈ 10 μg TEV protease per ≈ 1 mg of protein, followed by rocking at room temperature overnight. This sample was then applied directly to a 120 mL Superdex 75 gel filtration column that had been pre-equilibrated with 25 mmol/L Tris, pH 7.5, 100 mmol/L NaCl, 0.7 mol/L glycerol (5% (v/v)), and 1 mmol/L TCEP. The eluted fractions of monomeric FeoC were pooled and concentrated with a 4 mL Amicon 3 kg/mol (3 kDa) MWCO spin concentrator. To verify size, additional size-exclusion experiments were performed in a similar manner but with a 24 mL Superdex 75 column calibrated with low-molecular weight protein standards (MilliporeSigma). Protein concentration was determined using the Lowry assay, and purity was assessed via SDS-PAGE (acrylamide mass fraction of 15%) and Tris-tricine SDS-PAGE (acrylamide mass fraction gradient from 10% to 20%) analyses.

Anaerobic Reconstitution. Samples were reconstituted in an anaerobic chamber (Coy Laboratory Products, Grass Lake, MI) containing a N_2/H_2 atmosphere and operating at < 7 mg/m^3 (5 ppm) O_2. Briefly, protein was brought into the anaerobic chamber and allowed to equilibrate with the anaerobic chamber's atmosphere overnight at 6 °C with shaking. Protein was then diluted to 100 μmol/L in reconstitution buffer comprising 50 mmol/L MOPS, pH 7.5, 100 mmol/L NaCl, 1 mmol/L DTT, 0.7 mol/L glycerol (5% (v/v)). 10 mmol/L stock $FeCl_3$ was first titrated into the apo protein until up to 6 mole equivalents had been added with 10 min shaking at 6 °C between the addition of each mole equivalent of Fe^{+3}. 10 mmol/L stock Na_2S was then titrated into the iron-bound protein in the same manner. Afterwards, protein was equilibrated with $FeCl_3$ and Na_2S for ≈ 2 h at 6 °C with shaking. Particulate matter was removed by first centrifuging at 14000×*g*

anaerobically for 10 min at 4 °C and then by filtration through a filter with a 0.22 μm pore size. Excess iron and sulfide were removed by buffer exchanging using a 0.5 mL Amicon 3 kg/mol (3 kDa) MWCO spin concentrator at least four times into fresh 50 mmol/L MOPS, pH 7.5, 100 mmol/L NaCl, 1 mmol/L DTT, 0.7 mol/L glycerol (5% (v/v)). Iron contents were determined as described below.

Iron Content Determination. Iron content was determined spectrophotometrically using a modified version of the ferrozine assay.[35, 36] Briefly, protein was precipitated using 5 mol/L (50 % (v/v)) trichloroacetic acid (TCA). The supernatant was decanted and subsequently neutralized with saturated ammonium acetate. To this solution, excess ascorbic acid and 0.30 mmol/L ferrozine (final concentration) were added. Absorbance measurements of samples made in triplicate were taken at 562 nm. The concentration of Fe^{2+} was then determined assuming a Fe^{2+}-ferrozine complex with an extinction coefficient (ε_{562}) of ≈ 28 L mmol^{-1} cm^{-1} [36] (26.98 L mmol^{-1} cm^{-1} $\pm$ 0.96 L mmol^{-1} cm^{-1})[35], and these data were corrected against residual iron present in buffer constituents.

Electronic Absorption and Circular Dichroism Spectroscopies. Electronic absorption spectra were recorded at room temperature on a Cary 60 UV-visible spectrophotometer (Agilent). Samples were contained within a 1 cm UV-transparent cuvette, and data were acquired from 800 nm to 250 nm with the instrument set to a spectral bandwidth of 2 nm. Absorption studies designed to follow the oxidation of reconstituted FeoC were performed in two ways, both at room temperature. First, anaerobically reconstituted protein was buffer exchanged into 50 mmol/L MOPS, pH 7.5, 100 mmol/L NaCl, 1 mmol/L TCEP, 0.7 mol/L glycerol (5% (v/v)) and aliquoted into a UV-transparent cuvette and stoppered inside of an anaerobic chamber. Following removal from the anaerobic chamber, the stopper was removed, the cuvette was flushed with ambient atmosphere, and the oxidation process was monitored by scanning kinetics from 800 nm to 250 nm with spectra

accumulated every 6 s until reactivity appeared to cease (≈ 15 min to 20 min). Second, air-saturated buffer (25 mmol/L Tris, pH 7.5, 100 mmol/L NaCl, 0.7 mol/L glycerol (5 % (v/v)), and 1 mmol/L TCEP) was sealed inside of a container and brought into an anaerobic chamber. Buffer was mixed with protein in a 1:1 v:v ratio, also contained inside of a septum-sealed cuvette, using a gastight syringe. Once again, the oxidation process was monitored by scanning kinetics from 800 nm to 250 nm with spectra accumulated every 6 s until reactivity appeared to cease (≈ 5 min). Observed kinetic data (k_{obs}) were fitted to the following equation:

$$Abs_t = Abs_\infty + \alpha e^{-kt}$$

Circular dichroism (CD) spectra were recorded on a nitrogen-flushed Jasco J710 spectropolarimeter operating at room temperature. Samples were contained within a 1.0 cm quartz cuvette, and data were acquired from 400 nm to 190 nm with the instrument set to a spectral bandwidth of 1 nm. Plotted CD data represent the average of 5 scans.

EPR Spectroscopy. Samples containing ≈ 100 μmol/L to 600 μmol/L iron (final concentration) in buffer plus 3.6 mol/L ethylene glycol (20% (v/v)) were aliquoted either aerobically or anaerobically (as warranted) into standard quartz X-band EPR tubes with a 4 mm outer diameter and flash-frozen in $N_{2(l)}$. For whole-cell EPR experiments, cells bearing either the empty pET-45b(+) plasmid or one of the two expression plasmids (either MBP-*Ec*FeoC or MBP-*Kp*FeoC, with and without expression in the presence of IPTG) were grown in the same manner as previously described (*vide supra*). In order to remove adventitious metal bound to the cell surface, cell pellets were washed at least three times by repeated resuspension and centrifugation in cellular resuspension buffer to which 1 mmol/L EDTA had been added. After the final centrifugation step, cells were resuspended to a concentration of ≈ 1.5 g/mL in resuspension buffer without EDTA. The cell suspension was then aliquoted into standard quartz X-band EPR tubes with a 4 mm outer

diameter and flash-frozen in $N_{2(l)}$. Spectra were collected at temperatures indicated in the figure legend using a commercial EPR spectrometer system equipped with a high-sensitivity, TE-mode, CW resonator and commercial temperature-control unit. The uncertainty on the reported *g* values is 0.0005, using the manufacturer-reported field (0.08 mT) and frequency (0.00005 GHz) accuracies. The maximum, minimum and baseline-crossing points of peaks were used to determine magnetic field positions for *g* values. Calculated *g* values (from magnetic field values) agree with *g* values directly reported by the spectral analysis software provided with the commercial instrument to within 0.001.

X-ray Absorption Spectroscopy. Samples containing ≈ 0.5 mmol/L to 2 mmol/L iron (final concentration) in buffer plus 3.6 mol/L ethylene glycol (20% (v/v)) were aliquoted either aerobically or anaerobically (as warranted) into Lucite cells wrapped with Mylar tape, flash frozen in $N_{2(l)}$ and stored at −80 °C until data collection. X-ray absorption data was collected on beamlines 7-3 and 9-3 at the Stanford Synchrotron Radiation Lightsource (Menlo Park, CA) as replicates when possible. Extended X-ray absorption fine structure (EXAFS) of Fe (7210 eV) was measured using a Si 220 monochromator with crystal orientation $\phi = 90°$. Samples were measured as frozen aqueous glasses in 3.6 mol/L ethylene glycol (20% (v/v)) at 15 K, and the X-ray absorbance was detected as Kα fluorescence using either a 100-element (beamline 9-3) or 30-element (beamline 7-3) Canberra Ge array detector. A Z-1 metal oxide filter (Mn) and Soller slit assembly were placed in front of the detector to attenuate the elastic scatter peak. A sample-appropriate number of scans of a buffer blank were measured at the absorption edge and subtracted from the raw data to produce a flat pre-edge and eliminate residual Mn Kβ fluorescence of the metal oxide filter. Energy calibration was achieved by placing a Fe metal foil between the second and third ionization chamber. Data reduction and background subtraction were performed using EXAFSPAK.[37] The

data from each detector channel were inspected for drop outs and glitches before being included into the final average. EXAFS simulation was carried out using the program EXCURVE 9.2 as previously described.[38-40] The quality of the fits was determined using the least-squares fitting parameter, *F*, which is defined as:

$$F^2 = \frac{1}{N}\sum_{i=0}^{N} k^6(\chi_i^{theory} - \chi_i^{exp})^2$$

and is referred to as the fit index (FI).

Dynamic Light Scattering Studies. Intensity, volume, and number distributions relating to the diameters of apo and [4Fe-4S]-bound FeoC forms (assumed to be perfect spheres in solution) were analyzed by dynamic light scattering (DLS) spectroscopy. DLS measurements were performed at room temperature with a Malvern Zetasizer Nano ZS equipped with a 633 nm He–Ne laser and operating at an angle of 173°. Protein samples, typically ≈ 400 μmol/L to 900 μmol/L, were prepared anaerobically in a septum-stoppered low-volume quartz cuvette at room temperature. Data are the average of three replicate scans performed on at least two independent protein preparations. Dispersities (Đ) had prep-to-prep variations but were generally in a range of ≈ 0.1 to 0.2, indicating uniform dispersity, correlating well with our size-exclusion analyses (*vide supra*).

Results

Expression and purification of EcFeoC.

Due to the small size of *Ec*FeoC (≈ 9 kg/mol, 9 kDa), we needed to explore several methods to express and to purify this protein. Our initial approach was one in which we cloned the gene corresponding to *Ec*FeoC (Uniprot ID: P64638) into the IPTG-inducible pET-21a(+) expression plasmid with a cleavable, C-terminal $(His)_6$ tag (MW ≈ 10 kg/mol, 10 kDa). Despite exhaustive efforts to express this tagged protein, including multiple expression temperatures, times, and media, we were unable to observe appreciable accumulation of this expression construct in either the soluble or membrane-bound fractions within *E. coli* as the expression host. Therefore, we created a new expression construct encoding for a maltose-binding protein (MBP) fusion that we subcloned into the IPTG-inducible pET-45b(+) expression plasmid. This final expression construct encodes for an N-terminal $(His)_6$ tag tethered to MBP with a TEV protease site immediately preceding *Ec*FeoC (*i.e.*, H_2N-$(His)_6$-MBP-TEV-FeoC-COOH) (Fig. 2A). Expression of this construct was robust within *E. coli* under numerous conditions, and this construct was found chiefly within the soluble fraction of the cell lysate. We then took advantage of the MBP moiety of this construct for protein purification, and after a single round of affinity chromatography, we were able to purify our MBP-*Ec*FeoC fusion to high purity (estimated to be > 95%; Fig. 2) and excellent yields (> 100 mg/L of cell culture) (Fig. S1A).

After our initial round of purification, we isolated *Ec*FeoC from MBP by TEV protease cleavage and subsequent size-exclusion chromatography (SEC; Fig. 2B). After overnight incubation with the protease, complete cleavage of the starting protein construct was evident (Fig. S1A), yielding the nearly native *Ec*FeoC protein with a single additional Gly residue on the N-terminus. We then separated cleaved *Ec*FeoC from His-tagged MBP and TEV protease by size-

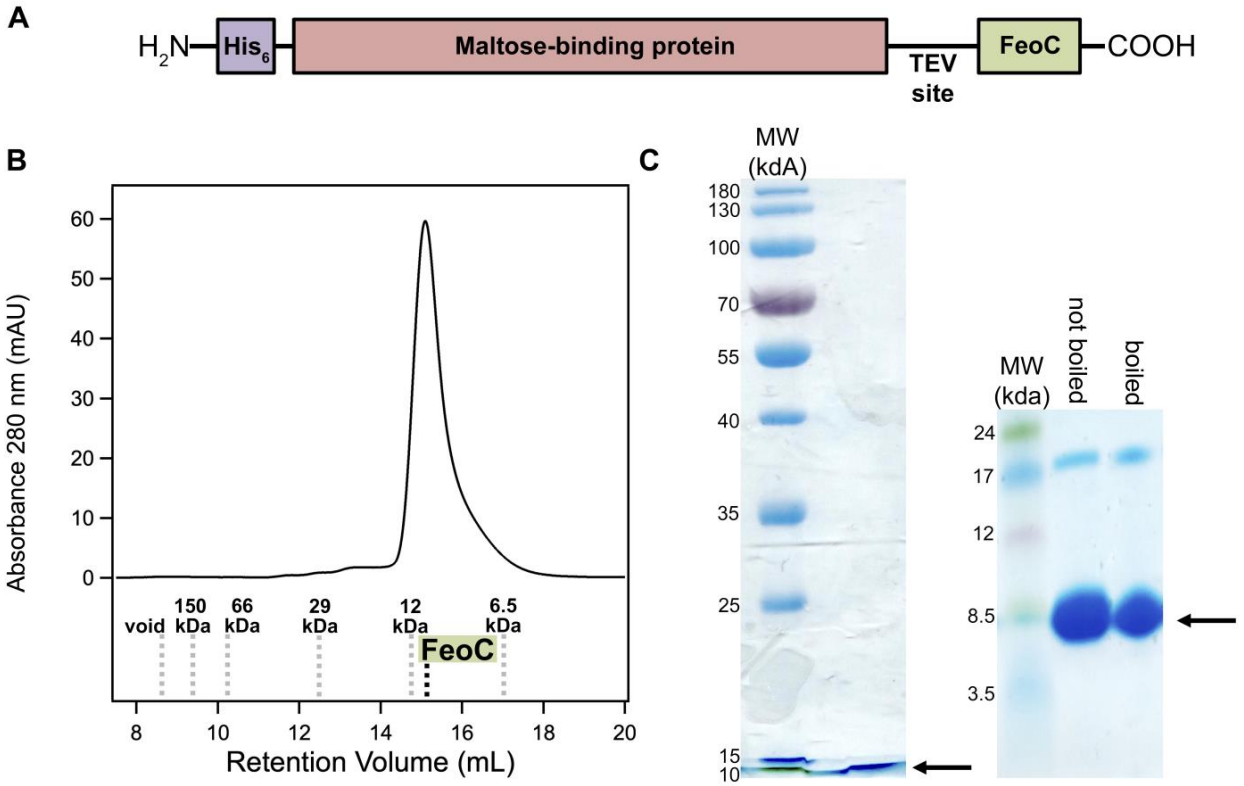

Figure 2. Construct design and purification of *Ec*FeoC. **A**. Because of poor native expression, *Ec*FeoC was expressed as a maltose-binding protein (MBP; salmon) fusion (MBP-*Ec*FeoC). On the N-terminus is encoded an additional $(His)_6$ tag (purple) for orthogonal purification. Preceding the *Ec*FeoC portion of the polypeptide (green) is an encoded TEV protease cleavage site. **B**. Cleaved, purified *Ec*FeoC is monomeric (≈ 9000 g/mol, 9 kDa) based on its gel-filtration retention volume on Superdex 75. The compared standards (K_{av} versus log MW, linearity R^2=0.97) are: blue dextran (void), alcohol dehydrogenase (150000 g/mol, 150 kDa), bovine serum albumin (66000 g/mol, 66 kDa), carbonic anhydrase (29000 g/mol, 29 kDa), cytochrome *c* (12000 g/mol, 12 kDa), and aprotinin (6500 g/mol, 6.5 kDa). **C**. SDS-PAGE analysis (acrylamide mass fraction of 15 %, left panel) and Tris-tricine gel analysis (gradient of acrylamide mass fraction from 10 % to 20 %, right panel), demonstrating *Ec*FeoC purity after cleavage and SEC. Black arrows indicate the location of the purified *Ec*FeoC. A small amount of dimeric *Ec*FeoC (≈ 18000 g/mol, 18 kDa) is observed in the Tris-tricine analysis at high protein concentration, but this dimeric species is only observed after freeze-thawing of the protein and cannot be dissociated by sample boiling.

exclusion chromatography (SEC) on Superdex 75 (Fig. 2B; Fig. S1B). This final step yielded highly pure, monomeric *Ec*FeoC in good yield (Fig. 2C). To verify that our cleaved *Ec*FeoC construct was not unfolded after TEV protease treatment and MBP separation, we measured its

far-UV circular dichroism (CD) spectrum, which displayed the expected mixture of α helices, β strands, and random coil, instead of an unfolded state (Fig. S2).

Aerobically isolated MBP-EcFeoC contains degradation products of a [4Fe-4S] cluster.

Aerobically-purified MBP-*Ec*FeoC expressed in unsupplemented LB medium bore a red-brown color that became increasingly more intense

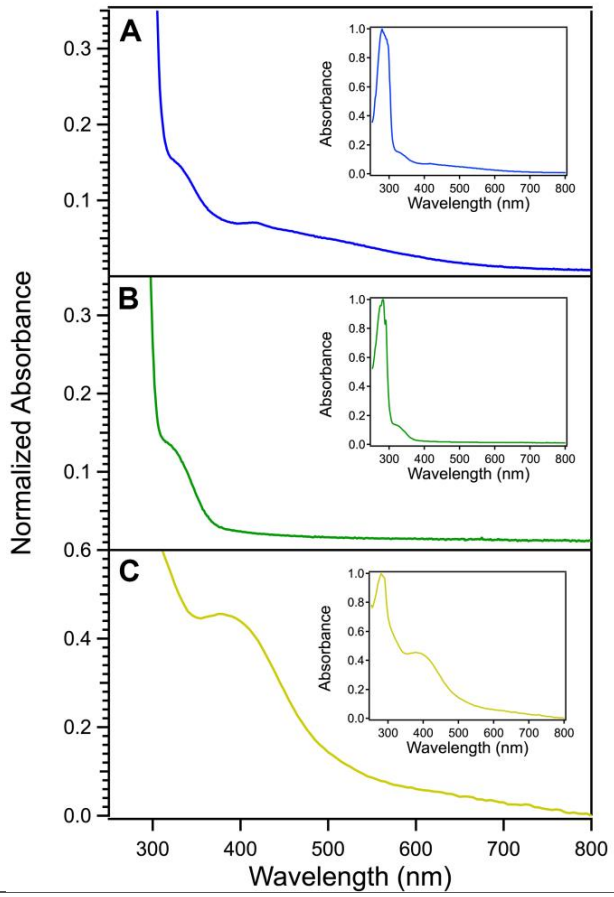

Figure 3. Electronic absorption spectroscopy of *Ec*FeoC species suggests the presence of [Fe-S] clusters. **A**. Absorption spectrum of the MBP-*Ec*FeoC fusion protein aerobically as-isolated. **B**. Absorption spectrum of the cleaved apo *Ec*FeoC protein. **C**. Absorption spectrum of the cleaved, anaerobically reconstituted *Ec*FeoC protein. Solutions were kept at room temperature in a UV-transparent cuvette, and protein concentrations were generally 1 μmol/L to 20 μmol/L. Sample **A** was in MBP elution buffer, sample **B** was in TEV cleavage buffer, and sample **C** was in anaerobic reconstitution buffer (see Materials and Methods). Absorption data are normalized to the most intense band corresponding to the protein absorbance (280 nm), and each inset displays the full spectrum of each sample.

during protein concentration, common to many [Fe-S] clusters. Metal analysis alone (iron content of (0.23 ± 0.02) ions per polypeptide, where the error is one standard deviation (confidence interval of 68.2%), derived from replicate experiments) was unable to assign the composition of the [Fe-S] cluster due to the presence of apo protein. However, most [Fe-S] clusters exhibit spectroscopic signatures that are indicative of the species that may be present.[41, 42] The MBP-*Ec*FeoC electronic absorption spectrum (Fig. 3A; λ_{max} of 330 nm and 418 nm with broad, overlapping peaks from 500 nm to 600 nm) bears a similarity to the previously reported spectrum of *Kp*FeoC,[34] which was also shown to bind an [Fe-S] cluster; however, while the spectrum of *Kp*FeoC had been attributed to the presence of an unusual oxygen-stable $[4Fe\text{-}4S]^{3+}$ HiPIP cluster,[34] the electronic absorption spectral signatures of both proteins are distinctly different from purely [4Fe-4S] or [2Fe-2S] clusters, potentially indicating multiple species.[43]

To probe the identity of the species in the MBP-*Ec*FeoC fusion construct, we analyzed the X-ray absorption (XAS) and electron paramagnetic resonance (EPR) spectra of this aerobically-isolated construct (Figs. 4A, 5A). Because both types of spectroscopy are sensitive to the nature, number, and types of nearest-neighbor ligands, as well as the oxidation state and number of unpaired electrons on the iron centers, these approaches can function to differentiate various cluster compositions from one another. Simulations of the extended X-ray absorption fine structure (EXAFS) data of MBP-*Ec*FeoC taken at the Fe edge reveal only S-based environments as the nearest neighbor ligands with an average distance of 0.226 nm ± 0.005 nm (2.26 Å ± 0.05 Å) (Fig. 4A and inset; Table 1), consistent with the presence of an [Fe-S] cluster. The involvement of any and all Cys residues must come from the *Ec*FeoC moiety (containing exactly four Cys residues: Cys^{56}, Cys^{61}, Cys^{64} and Cys^{70}, all numbered based on native *Ec*FeoC), as there are no other Cys residues within the fusion construct, and mutations encoding for Cys-Ala variant proteins analyzed

by Hsueh et al. have shown that these analogous residues play essential roles in Fe binding to the *Kp*FeoC homolog. Furthermore, there is no indication of O/N-nearest neighbor ligands,

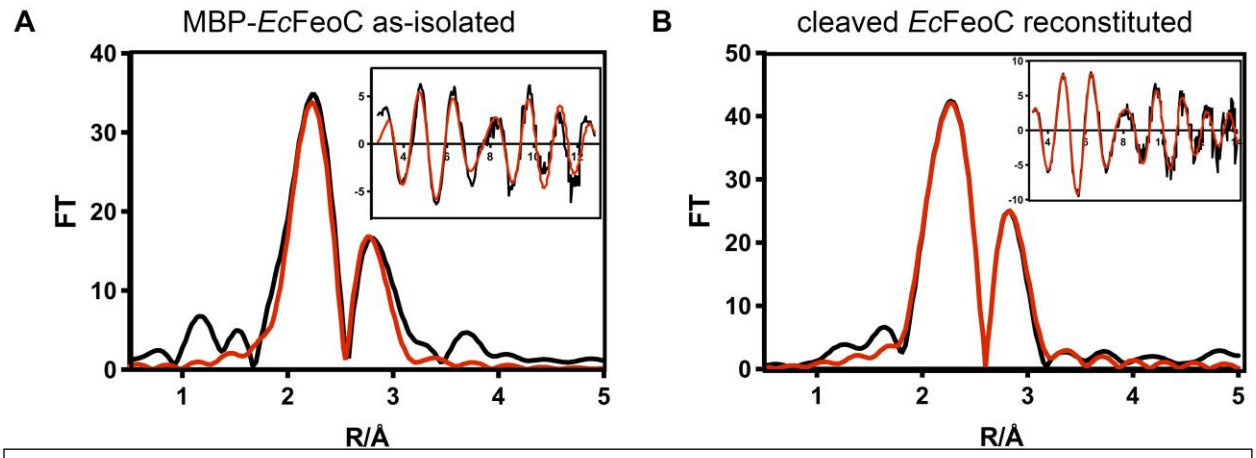

Figure 4. X-ray absorption spectroscopy (XAS) indicates the presence of [Fe-S] clusters in *Ec*FeoC. Fe K-edge X-ray absorption fine structure (EXAFS) and Fourier transforms of MBP-*Ec*FeoC (**A**) and anaerobically reconstituted *Ec*FeoC (**B**). For ease of interpretation, data are graphed as Fourier transform amplitude versus distance (R) in Å, where 1 Å = 0.1 nm. Black traces represent the experimental data, and red traces represent the simulations. Parameters used to generate the simulated spectra are listed in Table 1. Sample **A** was in 25 mmol/L Tris buffer, pH 7.5, 200 mmol/L NaCl, 10 mmol/L maltose, 3.6 mol/L ethylene glycol (20% (v/v)), and 0.7 mol/L glycerol (5% (v/v)). Sample **B** was in 50 mmol/L MOPS buffer, pH 7.5, 150 mmol/L NaCl, 10 mmol/L DTT, and 3.6 mol/L ethylene glycol (20% (v/v)).

precluding the involvement of the His tag in Fe binding. Furthermore, the presence of a fraction of a higher-order cluster is suggested, as long-range scattering interactions of an Fe-Fe vector are observed and fitted to a distance of 0.272 nm ± 0.005 nm (2.72 Å ± 0.05 Å) (Fig. 4A, Table 1). To probe the [Fe-S] compositions further, continuous wave (CW) X-band EPR spectroscopy was used, which indicates an admixture of different clusters. When analyzed over a range of 400 mT, the as-isolated, aerobic form of MBP-*Ec*FeoC has a single, strong EPR signal at $g \approx 4.3$ (Fig. 5A) at multiple temperatures, almost identical to the signal seen in oxidized rubredoxins[44] (*i.e.*, $[Fe^{3+}(Cys)_4]$), which is confirmed by our EXAFS data and indicates specific rather than adventitious interactions of Fe and the MBP-*Ec*FeoC fusion. To probe whether this rubredoxin-like species is operative inside of the recombinant host, we analyzed the whole-cell EPR spectrum

of *E. coli* cells grown aerobically and bearing either the empty plasmid or the expression plasmid encoding MBP-*Ec*FeoC, in the presence and absence of IPTG. Under all conditions tested, we

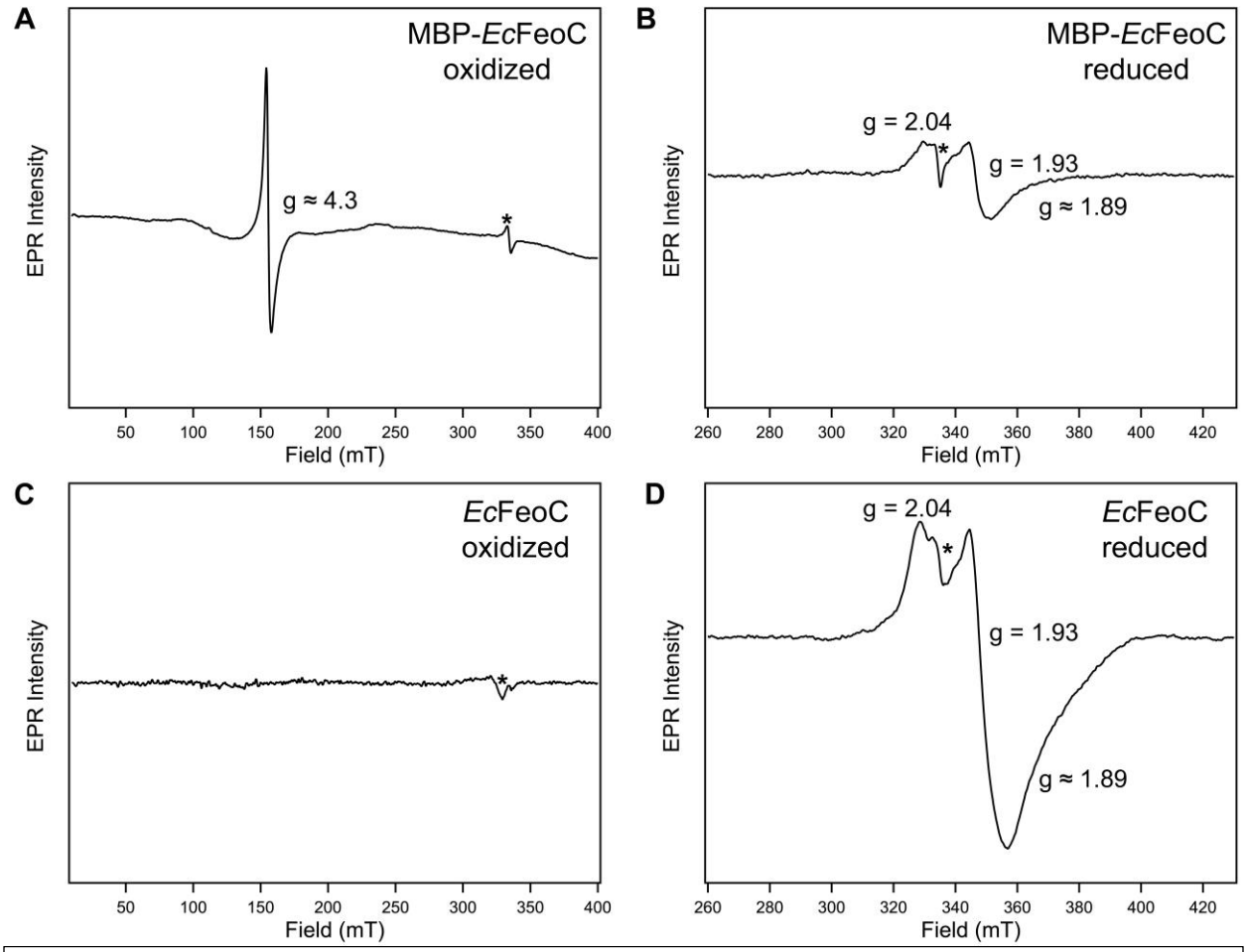

Figure 5. Electron paramagnetic resonance (EPR) spectroscopy indicates the identity of the observed [Fe-S] clusters in *Ec*FeoC. Continuous-wave (CW) X-band EPR spectra of MBP-*Ec*FeoC as-isolated (**A**), MBP-*Ec*FeoC reduced with sodium dithionite (**B**), cleaved and anaerobically-reconstituted *Ec*FeoC (**C**), and cleaved and anaerobically-reconstituted *Ec*FeoC reduced with sodium dithionite (**D**). Samples **A** and **B** were in 25 mmol/L Tris buffer, pH 7.5, 200 mmol/L NaCl, 10 mmol/L maltose, 3.6 mol/L ethylene glycol (20% (v/v) ethylene glycol), and 0.7 mol/L glycerol (5% (v/v) glycerol) ± 1 mmol/L sodium dithionite, respectively. Samples **C** and **D** were in 50 mmol/L MOPS buffer, pH 7.5, 150 mmol/L NaCl, 10 mmol/L DTT, and 3.6 mol/L ethylene glycol (20% (v/v) ethylene glycol) ± 1 mmol/L sodium dithionite, respectively. Samples **A** and **C** are plotted on identical scales, and samples **B** and **D** are plotted on identical scales. Spectral parameters were as follows: (**A**) 20 K, modulation amplitude = 0.5 mT, modulation frequency = 100 kHz, 1024 points, conversion time = 117.19 ms, microwave power = 9.5 mW, 4 scans (**B**) 20 K, modulation amplitude = 0.5 mT, modulation frequency = 100 kHz, 1024 points, conversion time = 87.89 ms, microwave power = 9.5 mW, 16 scans (**C**) 6 K, modulation amplitude = 0.5 mT, modulation frequency = 100 kHz, 1024 points; conversion time = 117.19 ms, microwave power = 4.7 mW, 1 scan (**D**) 6 K, modulation amplitude 0.5 mT, modulation frequency = 100 kHz, 1024 points, conversion time = 87.89 ms, microwave power = 1.9 mW, 16 scans. A cavity contaminant marked by an asterisk (*) at ≈ 335 mT (g ≈ 2.005) was observed even after background subtraction in all spectra.

observed no evidence for the signal at $g \approx 4.3$ (data not shown), indicating that this species is likely created during the aerobic purification process. Anaerobic addition of a solution of sodium dithionite rapidly bleached the visible electronic absorption spectrum of purified MBP-*Ec*FeoC (Fig. S3), caused the loss of this rubredoxin-like signal at $g \approx 4.3$, and gave rise to a weak rhombic EPR signal with *g* values of approximately 2.04, 1.93, and 1.89 (Fig. 5B). These values are similar to those observed for reduced $[4Fe\text{-}4S]^{+}$ clusters,[45, 46] indicating that some $[4Fe\text{-}4S]^{2+}$ (EPR-silent until reduction to the +1 state) is present even after aerobic purification. Importantly, we observe no spectral evidence for the presence of a HiPIP cluster in our MBP-*Ec*FeoC construct under oxidizing or reducing conditions for our purified protein or for our whole-cell analyses, as was previously suggested.[47] Taken together, it is clear that the aerobically-isolated MBP-*Ec*FeoC fusion purifies as an admixture of a rubredoxin-like cluster (likely deriving from decomposition of the higher-order [4Fe-4S] species) and a low amount of $[4Fe\text{-}4S]^{2+}$. Additionally, because our whole-cell EPR experiments show no discernible rhombic EPR signal attributable to the $[4Fe\text{-}4S]^{+}$ S=½ species, we surmise that the EPR-silent $[4Fe\text{-}4S]^{2+}$ cluster is present in this construct when expressed within the *E. coli* host prior to cell lysis and aerobic purification.

Anaerobic reconstitution of cleaved EcFeoC yields a $[4Fe\text{-}4S]^{2+}$ cluster.

Because [Fe-S] clusters may be oxygen sensitive and subject to oxidative degradation,[48] because we observed sub-stoichiometric loading of our MBP-*Ec*FeoC fusion, and because our spectral characterization suggested the presence of a degraded cluster, we chose to anaerobically reconstitute our cleaved *Ec*FeoC construct, which very closely mimics the native *Ec*FeoC form. During the cleavage process, the TEV protease and fusion construct are both mixed in a buffer containing EDTA; however, after cleavage and separation, *Ec*FeoC still retains a small amount of iron that was not chelated during this process (0.04 ions ± 0.02 ions per polypeptide), which gives

rise to the weak shoulder in the electronic absorption of the cleaved protein at $\lambda_{max} \approx 330$ nm (Fig, 3B). We then reconstituted the now-cleaved *Ec*FeoC (100 μmol/L final concentration) by incubation with up to 6 mole equivalents of Fe^{3+} (600 μmol/L final concentration) followed by 6 mole equivalents of S^{2-} (600 μmol/L final concentration) with the cleaved protein. After centrifugation, filtration, and several rounds of buffer exchanges, the reconstituted protein bore a golden yellow color with a single $\lambda_{max} \approx 400$ nm ($\varepsilon \approx 3{,}500$ $M^{-1}cm^{-1}$/molar equivalent iron) in the visible region. The electronic absorption spectrum of reconstituted cleaved *Ec*FeoC (Fig. 3C; Fig. S4) is distinct from the MBP-*Ec*FeoC (Fig. 3A), but bears a remarkable similarity to the [4Fe-4S]$^{2+}$-bound forms of FNR[49, 50] and Endo III[51]. Furthermore, the estimated molar absorptivity falls within the accepted range of proteins bound to a [4Fe-4S]$^{2+}$ cluster[52, 53], strongly suggesting a similar cluster composition bound to *Ec*FeoC. However, metal stoichiometry displayed prep-to-prep variation, with our best preps containing ≈ 3 Fe ions per polypeptide (2.6 ions ± 0.5 ions).

To confirm the presence of a [4Fe-4S]$^{2+}$ cluster and not a [3Fe-4S]$^{+}$ cluster, we then recorded and analyzed the XAS and EPR spectra of reconstituted *Ec*FeoC. The Fe edge EXAFS spectrum and best fits of anaerobically reconstituted *Ec*FeoC are shown in Fig. 4B and inset. Simulations of the EXAFS data again reveal only S-based environments as the nearest neighbor ligands with an average distance of 0.226 nm ± 0.005 nm (2.26 Å ± 0.05 Å) (Fig. 4B and inset, Table 1). The total Fe-S interactions are best fitted with a coordination number of 4, and long-range scattering interactions representing 1 Fe-Fe vector at 0.254 nm ± 0.005 nm (2.54 Å ± 0.05 Å) and 2 Fe-Fe vectors at 0.271 nm ± 0.005 nm (2.71 Å ± 0.05 Å) are now present (Fig. 4B and inset, Table 1), all consistent with the [4Fe-4S] designation and based on previous literature.[54] CW X-band EPR spectroscopy confirms this assignment and identifies the isolated form of anaerobically reconstituted *Ec*FeoC as a [4Fe-4S]$^{2+}$ cluster. The as-isolated form of reconstituted

*Ec*FeoC has no EPR signal when analyzed over a range of 400 mT (Fig. 5C) at multiple temperature ranges, indicating that the cluster is in its oxidized state (*i.e.*, $[4Fe\text{-}4S]^{2+}$) and that no $[3Fe\text{-}4S]^{+}$ nor any other EPR-active species are present. Anaerobic addition of a solution of sodium dithionite bleached the visible electronic absorption spectrum of reconstituted *Ec*FeoC and gave rise to only a narrow *S*=½ rhombic EPR signal with two distinct *g* values of approximately 2.04, 1.93, and a third *g* value at approximately 1.89 (Fig. 5D), very similar to other proteins that bind a $[4Fe\text{-}4S]^{+}$ cluster after chemical reduction.[45, 46] Thus, these data clearly indicate that anaerobically reconstituted *Ec*FeoC binds a redox-active $[4Fe\text{-}4S]^{2+/+}$ cluster (not a HiPIP cluster) and, based on our Fe-to-polypeptide stoichiometry, suggest ≈ 75 % cluster incorporation.

The EcFeoC $[4Fe\text{-}4S]^{2+}$ cluster is oxygen-sensitive.

Given the striking similarity of the spectral properties of *Ec*FeoC and the cluster-binding transcriptional regulator FNR, we wondered whether reconstituted *Ec*FeoC would be oxygen-sensitive in a similar manner. This curiosity was further stimulated by the previous suggestion the *Kp*FeoC bore a HiPIP cluster with long-lived oxygen insensitivity ($t_{½}$ ≈ 14 h; *i.e.*, ≈ 804 min).[34] After exchanging into a buffer containing TCEP to prevent competitive chelation of DTT, we removed samples of our anaerobically reconstituted *Ec*FeoC bearing $[4Fe\text{-}4S]^{2+}$ out of the glovebox and simply exposed the sample to ambient conditions while monitoring the electronic absorption features (Fig. S5A). Clearly divergent from *Kp*FeoC, upon exposure of *Ec*FeoC to air, we observed an isosbestic conversion of the electronic absorption features that indicated rapid (≈ 15 min for complete conversion) oxidative degradation of a $[4Fe\text{-}4S]^{2+}$ cluster (starting) to a distinctive $[2Fe\text{-}2S]^{2+}$ cluster (final),[50, 55, 56] nicely mirroring the spectral behavior of FNR under similar conditions, albeit more slowly.[50, 56] The kinetics of this process are complex and include an initial lag phase (Fig. S5B), prompting us to wonder whether this slowly, multi-phasic process

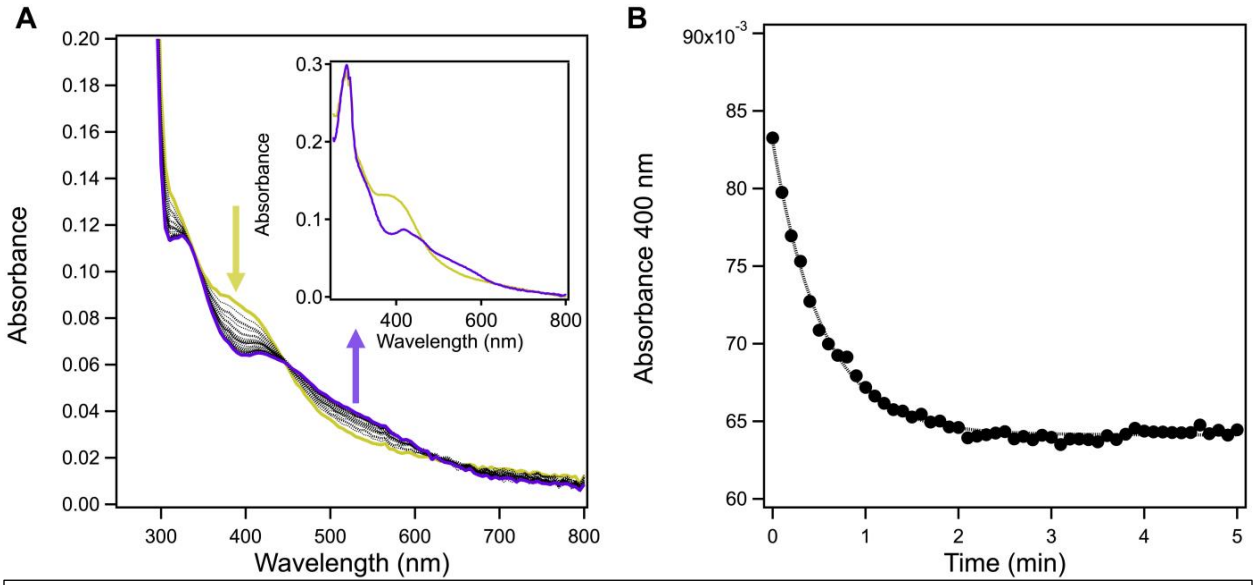

Figure 6. The $[4Fe\text{-}4S]^{2+}$ cluster of *Ec*FeoC is rapidly oxygen sensitive. **A**. Representative time course spectra of cleaved, anaerobically reconstituted *Ec*FeoC reacting with air-saturated buffer. Spectra were taken every 6 s (black, dotted) immediately after buffer mixing until reactivity stopped (≈ 5 min). The $[4Fe\text{-}4S]^{2+}$ spectral features (goldenrod) are rapidly lost and the appearance of the $[2Fe\text{-}2S]^{2+}$ spectral features rapidly appear (purple). The inset represents the plots of the two species before (goldenrod) and after (purple) reaction. The sample was in 50 mmol/L MOPS buffer, pH 7.5, 150 mmol/L NaCl, and 1 mmol/L TCEP at room temperature. **B**. Representative plot of the kinetic decay of the absorbance feature at 400 nm (closed circles), characteristic of the $[4Fe\text{-}4S]^{2+}$ cluster, and its fitted simulation (black dashed line), revealing a k_{obs} of (0.037 ± 0.010) s^{-1} and a $t_{½}$ of (19 ± 4.8) s when averaged over three replicates.

might be due to the limited oxygen diffusion into our previously anaerobic sample. To test this hypothesis, we repeated our cluster oxidation by mixing our anaerobic protein with air-saturated buffer in a 1:1 v:v ratio (estimated $[O_2]_{final} \approx 200$ μmol/L at room temperature[57]). We noted a more rapid conversion from the $[4Fe\text{-}4S]^{2+}$ to the $[2Fe\text{-}2S]^{2+}$ cluster form (≈ 5 min for complete conversion, Fig. 6A and inset), which we fitted to a single exponential decay (Fig. 6B) with a k_{obs} of (0.037 ± 0.010) s^{-1} representing a $t_{½}$ of (19 ± 4.8) s. These results are in excellent agreement with those observed for the oxidation of FNR under O_2-saturated conditions, in which a $k_{obs} \approx 0.04$ s^{-1} ($t_{½} \approx 10.2$ s) was reported.[56] Given the striking similarities between the two, we assume that the oxidative degradation of *Ec*FeoC follows a similar pattern as FNR in which the $[4Fe\text{-}4S]^{2+}$ cluster decomposition proceeds through a transient [3Fe-4S] cluster prior to formation of $[2Fe\text{-}2S]^{2+}$;[50]

however, we have yet to detect a spectroscopic signal diagnostic of a [3Fe-4S] cluster, which will require further investigation. Nevertheless, our data demonstrate that *Ec*FeoC [4Fe-4S]$^{2+}$ cluster is rapidly oxygen sensitive, strongly divergent from the previously reported behavior of *Kp*FeoC.[34]

KpFeoC also binds a redox-active, oxygen-sensitive [4Fe-4S] cluster

To rectify our results on *Ec*FeoC with those of the previous results on *Kp*FeoC, we cloned, expressed and purified an MBP-*Kp*FeoC fusion construct in an identical manner to that of MBP-*Ec*Feoc. The MBP-*Kp*FeoC construct expressed and purified to comparable final yields and purities as those of the MBP-*Ec*FeoC fusion (Fig. S6). Similarly, the purified MBP-*Kp*FeoC protein was colored (red-brown), had a sub-stoichiometric amount of iron bound (0.22 ions ± 0.19 ions per polypeptide), and an electronic absorption spectrum nearly identical to that of MBP-*Ec*FeoC (Fig. S7). The aerobically-purified MBP-*Kp*FeoC also displayed a strong, axial EPR signal at g = 4.30 with an additional weak signal at $g \approx 9.60$ (Fig. S8A) almost identical to the signal seen for MBP-*Ec*FeoC. Upon addition of sodium dithionite to the aerobically-purified MBP-*Kp*FeoC, the rubredoxin-like signal at g = 4.3 disappeared and gave rise to a weak rhombic EPR signal with g values of approximately 2.03, 1.94, and 1.90 (Fig. S8B), nearly identical to the [4Fe-4S]$^{+}$ seen in cleaved, anaerobically-reconstituted *Ec*FeoC. Additionally, whole-cell EPR experiments of overexpressed MBP-*Kp*FeoC show no discernible rhombic EPR signal attributable to the [4Fe-4S]$^{+}$ S=½ species (data not shown), leading us to the conclusion that the EPR-silent [4Fe-4S]$^{2+}$ is also operative for *Kp*FeoC within the cellular environment.

To test whether *Kp*FeoC would bind a redox-active [4Fe-4S] cluster like *Ec*FeoC, we sought to cleave and to reconstitute *Kp*FeoC anaerobically. Cleavage of MBP-*Kp*FeoC was accomplished in the same manner as MBP-*Ec*FeoC, and analysis of *Kp*FeoC on analytical Superdex 75 SEC yielded highly pure protein (Fig. S6) with an apparent MW of ≈ 12000 g/mol

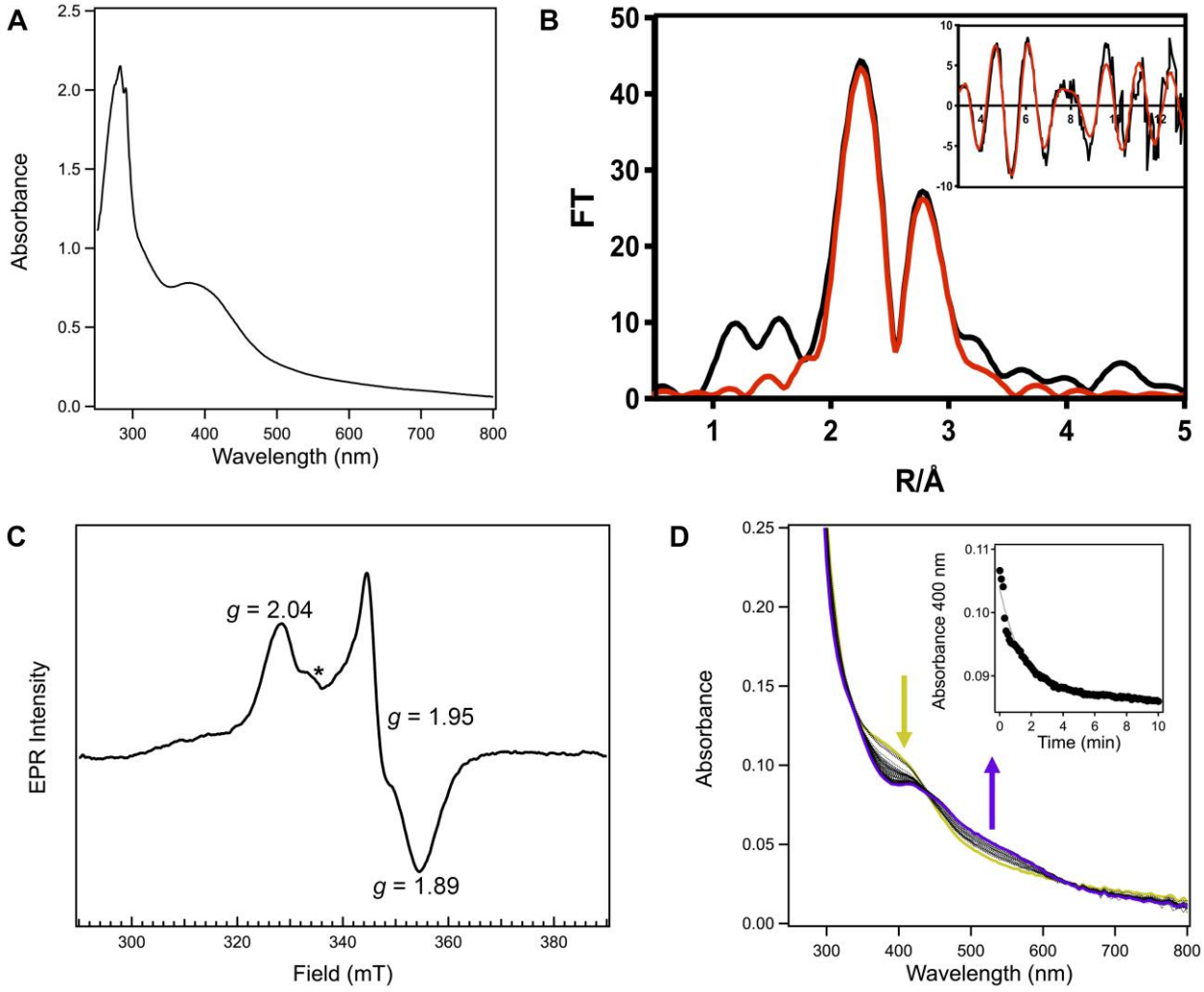

Figure 7. *Kp*FeoC also binds an redox-active, oxygen-sensitive [4Fe-4S] cluster. **A**. Absorption spectrum of the cleaved, anaerobically reconstituted *Kp*FeoC protein. Conditions were the same is in Figure 3C. **B**. Fe EXAFS and Fourier transforms of anaerobically reconstituted *Kp*FeoC. Conditions were the same as in Figure 4B. **C**. CW X-band EPR spectrum of cleaved and anaerobically-reconstituted *Kp*FeoC reduced with sodium dithionite. Sample conditions were the same as in Figure 5D. Data collection parameters were as follows: 10 K, modulation amplitude 0.5 mT, modulation frequency = 100 kHz, 1024 points, conversion time = 58.59 ms, microwave power = 0.47 mW, 16 scans. A cavity contaminant marked by an asterisk (*) at ≈ 335 mT (g ≈ 2.005) was observed even after background subtraction in all spectra. **D**. Representative time course spectra of cleaved, anaerobically reconstituted *Kp*FeoC reacting with air-saturated buffer. Spectra were taken every 6 s (black, dotted) immediately after buffer mixing until reactivity stopped. The $[4Fe\text{-}4S]^{2+}$ spectral features (goldenrod) are rapidly lost and the appearance of the $[2Fe\text{-}2S]^{2+}$ spectral features rapidly appear (purple). The inset represents the plot of the kinetic decay of the absorbance feature at 400 nm (closed circles), characteristic of the $[4Fe\text{-}4S]^{2+}$ cluster, and its fitted simulation (black dashed line), revealing a k_{obs} of (0.030 ± 0.020) s^{-1} and a $t_{½}$ of (34 ± 15) s when averaged over three replicates

(12 kDa). This higher MW deviates slightly from ideality when assuming a typical globular

protein, but it is expected for a protein with a highly unstructured and dynamic domain, like the wing of the winged-helix motif of *Kp*FeoC. Anaerobic reconstitution was performed in the same manner as cleaved *Ec*FeoC, resulting in a deeply golden-yellow protein with $\lambda_{max} \approx 400$ nm ($\varepsilon \approx$ 3,500 $M^{-1}cm^{-1}$/molar equivalent iron) (Fig. 7A and Fig. S9) with significantly increased iron content (1.77 ions per polypeptide ± 0.14 ions per polypeptide). This spectrum is again nearly identical to the $[4Fe\text{-}4S]^{2+}$-bearing proteins, which is confirmed by EXAFS and EPR analyses. Simulations of EXAFS data reveal 4 S-based environments as the nearest neighbor ligands with an average distance of 0.231 nm ± 0.005 nm (2.31 Å ± 0.05 Å) (Fig. 7B and inset, Table 1). Long-range scattering interactions representing 2 Fe-Fe vectors at 0.272 nm ± 0.005 nm (2.72 Å ± 0.05 Å) and 1 Fe-Fe vector at 0.285 nm ± 0.005 nm (2.85 Å ± 0.05 Å) are present (Fig. 7B and inset, Table 1), consistent with the [4Fe-4S] designation and based on previous literature, and suggesting a lower asymmetry in the geometry of this cubane-like cluster, distinct from *Ec*FeoC. Confirming this assignment, addition of sodium dithionite to the reconstituted, EPR-silent *Kp*FeoC protein (Fig. S8C) removed all visible electronic absorption spectral features and gave rise to a single, narrow rhombic EPR signal with distinct *g* values of 2.04, 1.95, and 1.89 (Fig. 7C), shifted slightly from those of *Ec*FeoC but still indicating the presence of only the $[4Fe\text{-}4S]^{+}$ cluster. Under no conditions tested did we observe any spectral features indicating the presence of the previously suggested HiPIP-like cluster. Rather, in our hands, reconstituted *Kp*FeoC clearly binds a redox-active $[4Fe\text{-}4S]^{2+/+}$ cluster akin to *Ec*FeoC.

We finally sought to examine if the reconstituted *Kp*FeoC [4Fe-4S] cluster would be sensitive to the presence of oxygen. To test whether this were the case with cleaved, anaerobically-reconstituted *Kp*FeoC, we again mixed our $[4Fe\text{-}4S]^{2+}$-bound form of *Kp*FeoC with air-saturated buffer and analyzed the electronic absorption signatures of the cluster. In a rapid manner mirroring

the behavior of *Ec*FeoC, we noted reactivity as the spectral features indicative of the $[4Fe\text{-}4S]^{2+}$ cluster were quickly converted to those of the $[2Fe\text{-}2S]^{2+}$ form (Fig. 7D). We fitted these data to a pseudo first-order decay with a k_{obs} of (0.030 ± 0.020) s^{-1} and extracted a $t_{½}$ of (34 ± 15) s (Fig. 7D inset), comparable to that of *Ec*FeoC. These results stand in marked contrast to the previous study of *Kp*FeoC, which demonstrated an estimated $t_{½} \approx 14$ h (*i.e.*, ≈ 804 min). Thus, it appears that anaerobically-reconstituted FeoCs may have generally oxygen-sensitive clusters, whereas the previous results may have been observing reactivity of a degraded form of the *Kp*FeoC cluster.

The FeoC [4Fe-4S] cluster alters protein conformation but not protein oligomerization.

Despite unambiguous evidence that both *Ec*FeoC and *Kp*FeoC bind $[4Fe\text{-}4S]^{2+}$ clusters, metal analyses suggested sub-optimal anaerobic reconstitution (≈ 75 % and ≈ 50 % reconstitution, respectively). While it is not uncommon to produce apo protein during chemical reconstitution, this stoichiometry could indicate that binding of the [4Fe-4S] cluster initiates dimerization (*i.e.*, one [4Fe-4S] cluster per dimer), which we considered. Our studies of cleaved, aerobic apo *Ec* and *Kp*FeoCs indicate that the proteins migrate via gel filtration with apparent molecular masses roughly consistent with monomeric protein under aerobic conditions and in the presence (or absence) of reductant. However, due to experimental limitations and the rapid sensitivity to oxygen of our anaerobically reconstituted $[4Fe\text{-}4S]^{2+}$ forms (*vide supra*), we could not repeat this experiment in the same manner. To circumvent this issue, we turned to dynamic light scattering (DLS), which we could adapt to anaerobic conditions in order to compare the size distribution of *Ec* and *Kp*FeoCs in solution prior and after anaerobic reconstitution.

The results of our DLS studies support a change in protein conformation upon cluster binding, but our data are inconsistent with a model of cluster-mediated dimerization. DLS analysis

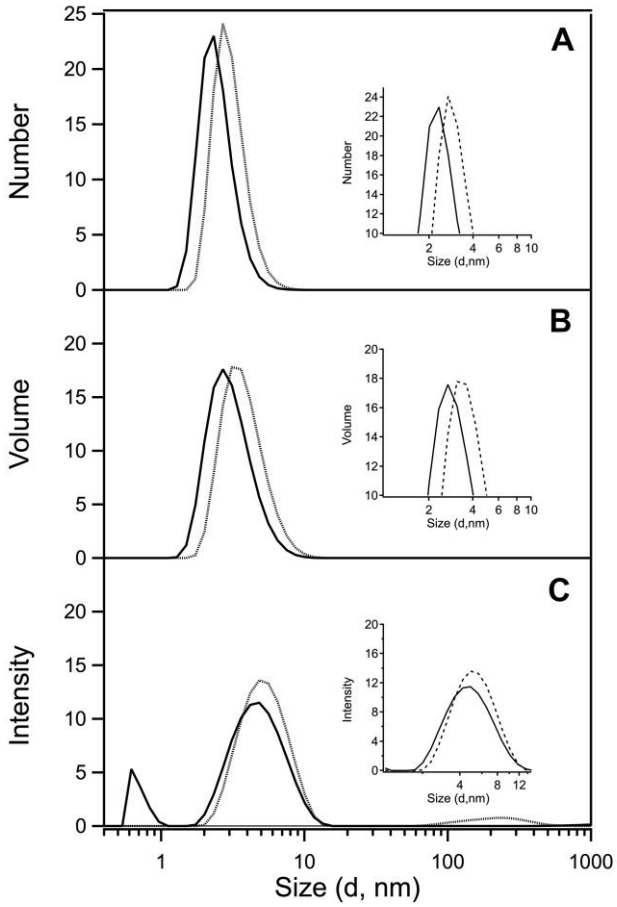

Figure 8. *Ec*FeoC does not dimerize in the presence of the $[4Fe\text{-}4S]^{2+}$ cluster. Representative dynamic light scattering (DLS) data of apo (dashed) and $[4Fe\text{-}4S]^{2+}$-bound forms (solid) of *Ec*FeoC plotted as number (**A**), volume (**B**), or intensity (**C**) versus globular diameter, clearly demonstrating the cluster-bound form assumes a more compact shape than the apo form of *Ec*FeoC. Samples were in 50 mmol/L MOPS buffer, pH 7.5, 150 mmol/L NaCl, and 1 mmol/L DTT at room temperature.

of cleaved *Ec*FeoC by intensity (Fig. 8C) indicates high monodispersity with only minimal aggregation. When calculated by volume (Fig. 8B) or by number (Fig. 8A), the size distribution is dominated by scattering of a narrow ensemble of particles < 10 nm in diameter. Based on number, the distribution of cleaved apo *Ec*FeoC in solution is calculated to have an ideal globular shape with a range of diameters ≈ 2.9 nm to 3.4 nm (29 Å to 34 Å). While it is known from NMR studies that the *Ec*FeoC protomer has an elongated rather than a globular shape (PDB ID 1XN7), this value is a useful benchmark to compare the behavior of the reconstituted protein. Even if a large

amount of surface were buried, one would expect dimerization to increase the size of the DLS particle distribution modestly after anaerobic reconstitution if cluster-mediated oligomerization were operative. In fact, we observe exactly the opposite: upon reconstitution to the $[4Fe\text{-}4S]^{2+}$ *Ec*FeoC form, the uniformity remains comparable (Fig. 8C), while the calculated size distributions by volume (Fig. 8B) or by number (Fig. 8A) *decrease* modestly. Calculated based on number, the globular diameter of the anaerobically-reconstituted *Ec*FeoC has contracted in size to ≈ 0.21 nm to 0.25 nm (21 Å to 25 Å). Similar behavior is observed for *Kp*FeoC (Fig. S10): When analyzed by number, the DLS signature of cleaved, apo *Kp*FeoC is dominated by a diameter distribution centered at 2.8 nm ± 0.66 nm (28 Å ± 6.6 Å) (Fig. S10, top panel). We then repeated the measurements with the [4Fe-4S]-bound form of *Kp*FeoC and found minimal changes in the DLS signature analyzed by number: holo *Kp*FeoC is dominated by a slightly contracted diameter distribution centered at 2.3 nm ± 0.68 nm (23 Å ± 6.8 Å). This behavior indicates only a modest change in the solution-state behavior of both apo and holo FeoCs, suggesting the protein slightly changes conformation but remains monomeric upon cluster binding.

We attempted to do the same measurement after exposure of $[4Fe\text{-}4S]^{2+}$ FeoCs to oxygen to generate the $[2Fe\text{-}2S]^{2+}$ forms; however, the analysis was hindered by the formation of an $FeS_{(s)}$ decomposition product of the oxidized $[4Fe\text{-}4S]^{2+}$ form that dominated the DLS measurements. Instead, we analyzed the more oxygen-stable $[2Fe\text{-}2S]^{2+}$ FeoC forms via SEC and noted a nearly identical retention volume (*i.e.*, size) to that of cleaved apo FeoCs prior to reconstitution (Fig. S11). Thus, our data indicate that FeoCs remain monomeric in all three oxidized forms studied here (apo, $[4Fe\text{-}4S]^{2+}$, and $[2Fe\text{-}2S]^{2+}$), consistent with FeoCs lacking any obvious dimerization domain, while it appears that binding of the $[4Fe\text{-}4S]^{2+}$ cluster compacts the conformation of cluster-bound FeoC compared to the apo form.

Discussion

In this work, we demonstrate that *Ec*FeoC binds an [Fe-S] cluster, and we have characterized the physical and electronic nature of this cluster extensively. When isolated aerobically, we show that the MBP-*Ec*FeoC fusion has combined spectral properties consistent with a mixture of redox-active $[4Fe\text{-}4S]^{2+/+}$ and rubredoxin-like clusters. We believe that the rubredoxin-like cluster derives from oxidative degradation of the [4Fe-4S] cluster during aerobic protein purification (Fig. 9), and this assertion is supported by a combination of electronic absorption, EPR, and X-ray absorption spectroscopies.

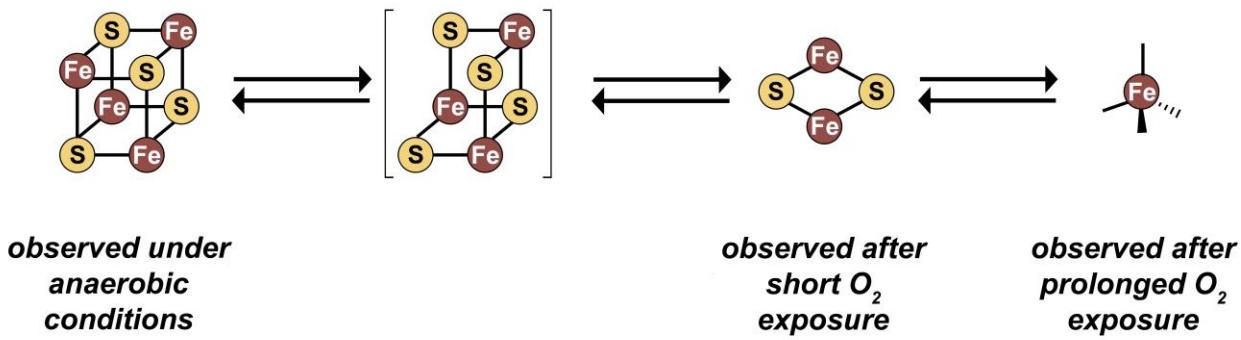

Figure 9. The observed forms of the redox-active, oxygen-sensitive cluster in *Ec*FeoC. Under strictly anaerobic conditions (such as those that may be operative within *E. coli* during anaerobic growth), a $[4Fe\text{-}4S]^{2+/+}$ cluster is observed. Upon reaction with oxygen-replete buffer, the $[4Fe\text{-}4S]^{2+}$ rapidly decays to a $[2Fe\text{-}2S]^{2+}$ cluster. After prolonged exposure to oxygen, a rubredoxin-like decay product (*i.e.*, $[Fe^{3+}(Cys)_4]$) is observed. Unlike FNR, we have yet to observe a $[3Fe\text{-}4S]^{+/0}$ cluster bound to *Ec*FeoC (indicated by the presence of brackets), but we surmise the transformation from $[4Fe\text{-}4S]^{2+}$ to $[2Fe\text{-}2S]^{2+}$ contains this transient species. This oxygen-responsive cluster disassembly may represent the behavior *Ec*FeoC undergoes *in vivo* during the organism's transition from anaerobic growth to aerobic growth.

Anaerobic reconstitution of the cleaved *Ec*FeoC demonstrates definitive spectral evidence for the binding of a redox-active $[4Fe\text{-}4S]^{2+/+}$ cluster, and we suggest this cluster composition is likely more operative within the prokaryotic cell under anaerobic and/or acidic conditions in which environmental Fe^{2+} is more prevalent and the *feo* operon is upregulated.[4, 7] This [4Fe-4S] cluster is also oxygen-sensitive, and our spectral data indicate a rapid (≈ 5 min for complete conversion)

oxygen-mediated decomposition of the $[4Fe\text{-}4S]^{2+}$ cluster to a $[2Fe\text{-}2S]^{2+}$ cluster. The observed *Ec*FeoC behavior is strongly reminiscent of the behavior of the transcriptional regulator FNR,[50, 56, 58] which also displays oxidative degradation of its [4Fe-4S] cluster as a transcriptional response. However, divergent from FNR, we do not observe cluster-mediated dimerization;[50] rather, our DLS data suggest that *Ec*FeoC remains monomeric but changes conformation upon cluster binding in solution, consistent with FeoCs lacking any obviously identifiable dimerization domains common to many transcriptional regulators.

In our hands, we observe nearly identical behavior between *Ec*FeoC and *Kp*FeoC, which stands in strong contrast to a previous spectroscopic study of *Kp*FeoC.[34] In the previous work, the authors demonstrated that a tagged form of *Kp*FeoC purified with a sub-stoichiometric (less than 10 %) admixture of multiple [Fe-S] cluster forms.[34] Based on EPR spectra and electronic absorption data, it was previously concluded that the as-isolated *Kp*FeoC cluster was enriched in an unusual $[4Fe\text{-}4S]^{3+}$ HiPIP form that could also access the $[4Fe\text{-}4S]^{2+/+}$ redox states, and that this HiPIP cluster could have functional relevance.[34] This conclusion seems extremely unusual for a γ-proteobacterium such as *K. pneumoniae*, as HiPIP clusters are commonly found in photosynthetic and denitrifying bacteria because of their extremely positive reduction potentials (*ca*. +50 mV to +500 mV).[59, 60] This highly-elevated redox potential is often used to drive electron transport within the respiratory and photosynthetic electron chains[60] and/or iron oxidation[61], precisely the opposite function of the Feo system, which maintains reduced iron stores. However, the electronic absorption and EPR data of *Kp*FeoC presented previously are inconsistent with any sort of [4Fe-4S] designation. For example, the aerobically-isolated electronic absorption of *Kp*FeoC is distinct from spectra of pure $[4Fe\text{-}4S]^{2+}$ or $[2Fe\text{-}2S]^{2+}$ clusters, and instead suggests the presence of a mixture of species similar to our MBP-*Ec*FeoC construct.[34] Furthermore, previously aerobically-

isolated *Kp*FeoC demonstrated an extremely weak, rhombic CW X-band EPR spectrum with g_1=2.060 and two overlapping values of g_2/g_3=2.007, with an increase in intensity with only a very modest shift upon dithionite reduction.[34] The shape of the spectrum and the narrow spread of the *g* values are more often observed in the common $[2Fe\text{-}2S]^{+}$ ferredoxin-like or $[4Fe\text{-}4S]^{+}$ cluster forms[45] rather than the much rarer $[4Fe\text{-}4S]^{3+}$ HiPIP form, which typically displays an axial spectrum of $g_1 \approx 2.12$ and $g_2/g_3 \approx 2.03$.[47] Only a narrow EPR window (≈ 280 mT to 400 mT) was previously reported for *Kp*FeoC, so it is unclear whether any additional features at $g \approx 4.3$ were present. Given the low percentage of cluster loading, the aerobic handling of a clearly oxygen-sensitive protein (as shown in this study), and the spectral features that are inconsistent with a [4Fe-4S] cluster, we believe that these data were previously used to incorrectly assign a HiPIP $[4Fe\text{-}4S]^{3+}$ cluster to *Kp*FeoC. Based on our data, we propose that a redox-active, oxygen-sensitive $[4Fe\text{-}4S]^{2+/+}$ species is a common feature of cluster-binding FeoCs.

Despite the noteworthy presence of a [4Fe-4S] cluster, the exact function of FeoC remains to be seen. Based on our current data and in conjunction with previous observations, we posit a working hypothesis in which the cluster-binding FeoCs may function as *in vivo* iron sensors. As FeoB-mediated ferrous iron import increases the labile ferrous iron pool within the cytosol, FeoC could receive iron directly from FeoB and become replete with its [4Fe-4S] cluster. Based on our data, this binding is associated with conformational changes of the FeoC polypeptide, most likely within the "wing" of the winged-helix motif, which is otherwise disordered (*i.e.*, extremely dynamic) in the apo form based on its NMR structure (Fig. 1C). This binding could also be reversible through an oxygen-mediated degradation pathway, as we observe in our *in vitro* studies.

This sensor hypothesis could be used to control Feo function at any of several levels. For example, FeoC could target the *feo* operon specifically for repression in lieu of upstream

dissociation of the global regulator FNR, which is driving transcription of multiple anaerobic processes across the cellular landscape.[58] Studies on the mutation of the *Y. pestis feoC* gene support this theory, as this mutant displayed overexpression of *feoA* and *feoB* genes,[62] and there is a promoter region that overlaps with *fnr* for which no regulator has been identified.[63] However, in our hands FeoC appears to remain monomeric in the presence of its cluster, which is unusual although not unheard of for transcriptional regulators.[64, 65] Alternatively, FeoC could function as part of the larger Feo complex, which could be dynamic under changing cellular conditions in cooperation with FeoB. Support that FeoC is part of the larger complex is found in the *Kp*NFeoB-*Kp*FeoC co-crystal structure (although the [Fe-S] cluster is absent)[66], and in studies on *V. cholerae* Feo system, that have shown that FeoA/B/C interact[25, 67] (although *Vc*FeoC is one of only a handful of FeoCs that lack the necessary cluster-binding residues). Finally, cluster binding could control the targeting of the Feo proteins for proteolytic degradation, as has been suggested based on studies in *S. enterica*.[68, 69] As it stands, it is difficult to rule out any of these possible functions. However, our ability to produce stable, cluster-bound FeoCs in the absence of oxygen has now set the stage to probe whether interactions with DNA, RNA, or other components of the Feo system may be regulated functionally by the oxidation state and composition of the [Fe-S] cluster, representing an exciting avenue of future research.

Acknowledgements

This work was supported by NSF CAREER grant 1844624 (A. T. S.), NIH-NIGMS grant R35 GM133479 (A. T. S.), and in part by NIH-NIGMS grant T32 GM066706 (A. E. S.). Sequence searches utilized both database and analysis functions of the Universal Protein Resource (UniProt) Knowledgebase and Reference Clusters (http://www.uniprot.org) and the National Center for Biotechnology Information (http://www.ncbi.nlm.nih.gov/). Use of the Stanford Synchrotron Radiation Lightsource, SLAC National Accelerator Laboratory, is supported by the U.S. Department of Energy, Office of Science, Office of Basic Energy Sciences under Contract No. DE-AC02-76SF00515. The SSRL Structural Molecular Biology Program is supported by the DOE Office of Biological and Environmental Research, and by the National Institutes of Health, National Institute of General Medical Sciences (including P41 GM103393).

The authors declare no competing financial interests.

Supporting Information

Supporting information is available free of charge on the ACS publication website:

SDS-PAGE and SEC analyses of MBP-*Ec*FeoC prior to and post cleavage (Fig. S1)

Far-UV CD spectra of cleaved, apo *Ec*FeoC (Fig. S2)

Electronic absorption spectra of as-isolated MBP-*Ec*FeoC prior and post reaction with sodium dithionite (Fig. S3)

Molar absorptivity data of cleaved, reconstituted $[4Fe\text{-}4S]^{2+}$ *Ec*FeoC (Fig. S4)

Spectral and kinetics data of oxygen-sensitive $[4Fe\text{-}4S]^{2+}$ *Ec*FeoC after exposure to ambient conditions (Fig. S5)

SDS-PAGE analysis of MBP-*Kp*FeoC prior to and post cleavage (Fig. S6)

Electronic absorption spectrum of as-isolated MBP-*Kp*FeoC prior to cleavage (Fig. S7)

CW X-band EPR spectra of as-isolated MBP-*Kp*FeoC prior to and post reduction with sodium dithionite, as well as cleaved, reconstituted $[4Fe\text{-}4S]^{2+}$ *Kp*FeoC prior to reduction with sodium dithionite (Fig. S8)

Molar absorptivity data of cleaved, reconstituted $[4Fe\text{-}4S]^{2+}$ *Kp*FeoC (Fig. S9)

DLS data on apo and cleaved, reconstituted $[4Fe\text{-}4S]^{2+}$ *Kp*FeoC (Fig. S10)

SEC analyses of FeoC after cluster conversion of $[4Fe\text{-}4S]^{2+}$ to $[2Fe\text{-}42]^{2+}$ (Fig. S11)

Accession Codes

*Ec*FeoC: Uniprot identifier P64638

*Kp*FeoC: Uniprot identifier B5XTS6

*Ec*MBP: Uniprot identifier P0AEX9

References

[1] Andrews, S. C., Robinson, A. K., and Rodríguez-Quiñones, F. (2003) Bacterial iron homeostasis, *FEMS Microbiol. Rev. 27*, 215-237.

[2] Ganz, T. (2008) Iron homeostasis: fitting the puzzle pieces together, *Cell Metab. 7*, 288-290.

[3] Coffey, R., and Ganz, T. (2017) Iron homeostasis: an anthropocentric perspective, *J. Biol. Chem. 292*, 12727-12734.

[4] Velayudhan, J., Hughes, N. J., McColm, A. A., Bagshaw, J., Clayton, C. L., Andrews, S. C., and Kelly, D. J. (2000) Iron acquisition and virulence in *Helicobacter pylori*: a major role for FeoB, a high-affinity ferrous iron transporter, *Mol. Microbiol. 37*, 274-286.

[5] Wilks, A., and Burkhard, K. A. (2007) Heme and virulence: how bacterial pathogens regulate, transport and utilize heme, *Nat. Prod. Rep. 24*, 511-522.

[6] Reinhart, A. A., and Oglesby-Sherrouse, A. G. (2016) Regulation of *Pseudomonas aeruginosa* virulence by distinct iron sources, *Genes 7*, E126.

[7] Sestok, A. E., Linkous, R. O., and Smith, A. T. (2018) Toward a mechanistic understanding of Feo-mediated ferrous iron uptake, *Metallomics 10*, 887-898.

[8] Cartron, M. L., Maddocks, S., Gillingham, P., Craven, C. J., and Andrews, S. C. (2006) Feo-Transport of ferrous iron into bacteria, *Biometals 19*, 143-157.

[9] Hantke, K. (1987) Ferrous iron transport mutant in *Escherichia coli* K12, *FEMS Microbiol. Lett. 44*, 53-57.

[10] Smith, A. T., and Sestok, A. E. (2018) Expression and Purification of Functionally Active Ferrous Iron Transporter FeoB from *Klebsiella pneumoniae, Protein Expr. Purif. 142*, 1-7.

[11] Sassone-Corsi, M., Chairatana, P., Zheng, T., Perez-Lopez, A., Edwards, R. A., George, M. D., Nolan, E. M., and Raffatellu, M. (2016) Siderophore-based immunization strategy to inhibit growth of enteric pathogens, *Proc. Natl. Acad. Sci. U.S.A. 113*, 13462-13467.

[12] Miethke, M., and Marahiel, M. A. (2007) Siderophore-Based Iron Acquisition and Pathogen Control, *Microbiol. Mol. Biol. Rev. 71*, 413-451.

[13] Wandersman, C., and Delepelaire, P. (2004) Bacterial Iron Sources: From Siderophores to Hemophores, *Annu. Rev. Microbiol. 58*, 611-647.

[14] Kim, H., Lee, H., and Shin, D. (2012) The FeoA protein is necessary for the FeoB transporter to import ferrous iron, *Biochem. Biophys. Res. Com. 423*, 733-738.

[15] Dashper, S. G., Ang, C. S., Veith, P. D., Mitchell, H. L., Lo, A. W., Seers, C. A., Walsh, K. A., Slakeski, N., Chen, D., Lissel, J. P., Butler, C. A., O'Brien-Simpson, N. M., Barr, I. G., and Reynolds, E. C. (2009) Response of *Porphyromonas gingivalis* to heme limitation in continuous culture, *J. Bacteriol. 191*, 1044-1055.

[16] Dashper, S. G., Butler, C. A., Lissel, J. P., Paolini, R. A., Hoffmann, B., Veith, P. D., O'Brien-Simpson, N. M., Snelgrove, S. L., Tsiros, J. T., and Reynolds, E. C. (2005) A novel *Porphyromonas gingivalis* FeoB plays a role in manganese accumulation, *J. Biol. Chem. 280*, 28095-28102.

[17] Pérez, N., Johnson, R., Sen, B., and Ramakrishnan, G. (2016) Two parallel pathways for ferric and ferrous iron acquisition support growth and virulence of the intracellular pathogen *Francisella tularensis* Schu S4, *MicrobiologyOpen 5*, 453-468.

[18] Sankari, S., and O'Brian, M. R. (2016) The *Bradyrhizobium japonicum* ferrous iron transporter FeoAB is required for ferric iron utilization in free living aerobic cells and for symbosis, *J. Biol. Chem. 291*, 15653-15662.

[19] Stojiljkovic, I., Cobeljic, M., and Hantke, K. (1993) *Escherichia coli* K-12 ferrous iron uptake mutants are impaired in their ability to colonize the mouse intestine, *FEMS Microbiol. Lett. 108*, 111-115.

[20] Tsolis, R. M., Baumler, A. J., Heffron, F., and Stojiljkovic, I. (1996) Contribution of TonB- and Feo-mediated iron uptake to growth of *Salmonella typhimurium* in the mouse, *Infect. Immun. 64*, 4549-4556.

[21] Naikare, H., Palyada, K., Panciera, R., Marlow, D., and Stintzi, A. (2006) Major Role for FeoB in *Campylobacter jejuni* Ferrous Iron Acquisition, Gut Colonization, and Intracellular Survival, *Infect. Immun. 74*, 5433-5444.

[22] Kammler, M., Schön, C., and Hantke, K. (1993) Characterization of the ferrous iron uptake system of *Escherichia coli*, *J. Bacteriol. 175*, 6212-6219.

[23] Thomas-Charles, C. A., Zheng, H., Palmer, L. E., Mena, P., Thanassi, D. G., and Furie, M. B. (2013) FeoB-mediated uptake of iron by *Francisella tularensis*, *Infect. Immun. 81*, 2828-2837.

[24] Runyen-Janecky, L. J., Reeves, S. A., Gonzales, E. G., and Payne, S. M. (2003) Contribution of the *Shigella flexneri* Sit, Iuc, and Feo iron acquisition systems to iron acquisition in vitro and in cultured cells, *Infect. Immun. 71*, 1919-1928.

[25] Weaver, E. A., Wyckoff, E. E., Mey, A. R., Morrison, R., and Payne, S. M. (2013) FeoA and FeoC are essential components of the *Vibrio cholerae* ferrous iron uptake system, and FeoC interacts with FeoB, *J. Bacteriol. 195*, 4826-4835.

[26] Perry, R. D., Mier Jr., I., and Fetherston, J. D. (2007) Roles of the Yfe and Feo transporters of *Yersinia pestis* in iron uptake and intracellular growth, *Biometals 20*, 699-703.

[27] Cornelis, P., and Dingemans, J. (2013) *Pseudomonas aeruginosa* adapts its iron uptake strategies in function of the type of infections, *Front. Cell. Infect. Microbiol. 3*, 1-7.

[28] Minandri, F., Imperi, F., Frangipani, E., Bonchi, C., Visaggio, D., Facchini, M., Pasquali, P., Brangozi, A., and Visca, P. (2016) Role of the iron uptake systems in *Pseudomonas aeruginosa* virulence and airway infection, *Infect. Immun. 84*, 2324-2335.

[29] Hunter, R. C., Asfour, F., Dingemans, J., Osuna, B. L., Samad, T., Malfroot, A., Cornelis, P., and Newman, D. K. (2013) Ferrous iron is a significant component of bioavailable iron in cystic fibrosis airways, *mBio 4*, e00557-00513.

[30] Banin, E., Vasil, M. L., and Greenberg, E. P. (2005) Iron and *Pseudomonas aeruginosa* biofilm formation, *Proc. Natl. Acad. Sci. U.S.A. 102*, 11076-11087.

[31] Singh, P. K., Parsek, M. R., Greenberg, E. P., and Welsh, M. J. (2002) A component of innate immunity prevents bacterial biofilm development, *Nature 417*, 552-555.

[32] Lau, C. K. Y., Krewulak, K. D., and Vogel, H. J. (2016) Bacterial ferrous iron transport: the Feo system, *FEMS Microbiol. Rev. 40*, 273-298.

[33] Hung, K.-W., Juan, T.-H., Hsu, Y.-L., and Huang, T. H. (2012) NMR structure note: the ferrous iron transport protein C (FeoC) from *Klebsiella pneumoniae J. Biolmol. NMR 53*, 161-165.

[34] Hsueh, K.-L., Yu, L.-K., Chen, Y.-H., Cheng, Y.-H., Hsieh, Y.-C., Ke, S.-c., Hung, K.-W., Chen, C.-J., and Huang, T.-H. (2013) FeoC from *Klebsiella pneumoniae* Contains a [4Fe-4S] Cluster, *J. Bacteriol. 195*, 4726-4734.

[35] Riemer, J., Hoepken, H. H., Czerwinska, H., Robinson, S. R., and Dringen, R. (2004) Colorimetric ferrozine-based assay for the quantitation of iron in cultured cells, *Anal. Biochem. 331*, 370-375.

[36] Jeitner, T. M. (2014) Optimized ferrozine-based assay for dissolved iron, *Anal. Biochem. 454*, 36-37.

[37] George, G. N. (1995) EXAFSPAK, Stanford Synchrotron Radiation Laboratory, Menlo Park, CA.

[38] Binsted, N., and Hasnain, S. S. (1996) State-of-the-art analysis of whole X-ray absorption spectra, *J. Synchrotron. Radiat. 3*, 185-196.

[39] Gurman, S. J., Binsted, N., and Ross, I. (1984) A rapid, exact curved-wave theory for EXAFS calculations, *J. Phys. C. 17*, 143-151.

[40] Gurman, S. J., Binsted, N., and Ross, I. (1986) A rapid, exact, curved-wave theory for EXAFS calculations. II. The multiple-scattering contributions, *J. Phys. C. 19*, 1845-1861.

[41] Crack, J. C., Green, J., Thomson, A. J., and Le Brun, N. E. (2014) Iron-sulfur clusters as biological sensors: the chemistry of reastions with moleculer oxygen and nitric oxide, *Acc. Chem. Res. 47*, 3196-3205.

[42] Johnson, D. C., Dean, D. R., Smith, A. D., and Johnson, M. K. (2005) Structure, function, and formation of biological iron-sulfur clusters, *Annu. Rev. Biochem. 74*, 247-281.

[43] Ugulava, N. B., Gibney, B. R., and Jarrett, J. T. (2001) Biotin synthase contains two distinct iron-sulfur cluster binding site: chemical and spetroelecrochemical analysis of iron-sulfur cluster interconversions, *Biochemistry 40*, 8343-8351.

[44] Peisach, J., Blumberg, B., Lode, E. T., and Coon, M. J. (1971) An analysis of the electron paramagneitc resonance spectrum of *Pseudomonas oleovorans* rubredoxin. A method for determinsation of the the ligands of ferric iron in completely rhombic sites, *J. Biol. Chem. 246*, 5877-5881.

[45] Guigliarelli, B., and Bertrand, P. (1999) Application of EPR spectroscopy to the structural and functional study of iron-sulfur proteins, *Adv. Inorg. Chem. 47*, 421-497.

[46] Cammack, R. (1992) Iron-sulfur clusters in enzymes: themes and variations, *Adv. Inorg. Chem. 38*, 281-322.

[47] Priem, A. H., Klaassen, A. A. K., Reijerse, E. J., Meyer, T. E., Luchinat, C., Capozzi, F., Dunham, W. R., and Hagen, W. R. (2005) EPR analysis of multiple forms of $[4Fe\text{-}4S]^{3+}$ clusters in HiPIPs, *J. Biol. Inorg. Chem. 10*, 417-424.

[48] Imlay, J. A. (2006) Iron-sulphur clusters and the problem with oxygen, *Mol. Microbiol. 59*, 1073-1082.

[49] Green, J., Bennet, B., Jordan, P., Ralph, E. T., Thomson, A. J., and Guest, J. R. (1996) Reconstitution of the [4Fe-4S] cluster in FNR and demonstration of the aerobic-anaerobic transcription switch *in vitro*, *Biochem. J. 316*, 887-892.

[50] Crack, J. C., Stapleton, M. R., Green, J., Thomson, A. J., and Le Brun, N. E. (2014) Influence of association state and DNA binding on the O_2-reactivity of [4Fe-4S] fumarate and nitrate reduction (FNR) regulation, *Biochem. J. 463*, 83-92.

[51] Tse, E. C. M., Zwang, T. J., and Barton, J. K. (2017) The oxidation state of [4Fe4S] clusters modulates the DNA-binding affinity of DNA repair proteins, *J. Am. Chem. Soc. 139*, 12784-12792.

[52] Jakimowicz, P., Cheesman, M. R., Bishai, W. R., Chater, K. F., Thomson, A. J., and Buttner, M. J. (2005) Evidence that the *Streptomyces* developmental protein WhiD, a member of the WhiB family, binds a [4Fe-4S] cluster, *J. Biol. Chem. 280*, 8309-8315.

[53] Crack, J. C., den Hengst, C. D., Jakimowicz, P., Subramaniam, S., Johnson, M. K., Buttner, M. J., Thomson, A. J., and Le Brun, N. E. (2009) Characterization of [4Fe-4S]-containing and cluster-free forms of *Streptomyces* WhiD, *Biochemistry 48*, 12252-12264.

[54] Silver, S. C., Gardenghi, D. J., Naik, S. G., Shepard, E. M., Huynh, B. H., Szilagyi, R. K., and Broderick, J. B. (2014) Combined Mössbauer spectroscopic, multi-edge X-ray absorption spectroscopic, and density functional theoretical study of the radical SAM enzyme spore photoproduct lyase, *J. Biol. Inorg. Chem. 19*, 465-483.

[55] Rajakovich, L. J., Nørgaard, H., Warui, D. M., Chang, W.-c., Li, N., Booker, S. J., Krebs, C., Bollinger, J., J. Martin, and Pandelia, M.-E. (2015) Rapid reduction of the diferric-peroxyhemiacetal intermediate in aldehyde-deformylating oxygenase by a cyanobacterial ferredoxin: evidence for a free-radical mechanism, *J. Am. Chem. Soc. 137*, 11695-11709.

[56] Sutton, V. R., Mettert, E. L., Beinert, H., and Kiley, P. J. (2004) Kinetic analysis of the oxidative conversion of the $[4Fe\text{-}4S]^{2+}$ cluster of FNR to a $[2Fe\text{-}2S]^{2+}$ cluster, *J. Bacteriol. 186*, 8018-8025.

[57] Reynafarje, B., Costa, L. E., and Lehninger, A. L. (1985) O_2 solubility in aqueous media determined by a kinetic method, *Anal. Biochem. 145*, 406-418.

[58] Crack, J., Green, J., and Thomson, A. J. (2004) Mechanism of Oxygen Sensing by the Bacterial Transcription Factor Fumarate-Nitrate Reduction (FNR), *J. Biol. Chem. 279*, 9278-9286.

[59] Tedro, S. M., Meyer, T. E., Bartsch, R. G., and Kamen, M. D. (1981) Primary structures of high potential, four-iron-sulfur ferredoxins from the purple sulfur photosynthetic bacteria, *Thiocapso roseopersicina* and *Chromatium gracile*, *J. Biol. Chem. 256*, 731-735.

[60] Bonora, P., Principi, I., Monti, B., Ciurli, S., Zannoni, D., and Hochkoeppler, A. (1999) On the role of high-potential iron-sulfur proteins and cytochromes in the respiratory chain of two facultative phototrophs, *Biochim. Biophys. Acta, Bioenergetics 1410,* 51-60.

[61] Ilbert, M., and Bonnefoy, V. (2013) Insight into the evolution of the iron oxidation pathways, *Biochim. Biophys. Acta, Bioenergetics 1827,* 161-175.

[62] Guo, J., Nair, M. K. M., Galván, E. M., Liu, S.-L., and Schifferli, D. M. (2011) Tn5AraOut mutagenesis for the identification of *Yersinia pestis* genes involved in resistance towards cationic antimicrobial peptides, *Microb. Path. 51,* 121-132.

[63] O'Connor, L., Fetherston, J. D., and Perry, R. D. (2017) The *feoABC* locus of *Yersinia pestis* likely has two promoters causing unique iron regulation, *Front. Cell. Infect. Microbiol. 7,* eCollection 2017.

[64] Feng, L., Chen, Z., Hu, Y., and Chen, S. (2016) Genome-wide characterization of monomeric transcriptional regulators in *Mycobacterium tuberculosis, Microbiology 162,* 889-897.

[65] Richet, E., and Raibaud, O. (1987) Purification and properties of the MalT protein, the transcription activator of the *Escherichia coli* maltose regulon, *J. Biol. Chem. 262,* 12647-12653.

[66] Hung, K.-W., Tsai, J.-Y., Juan, T.-H., Hsu, Y.-L., Hsiao, C.-D., and Huang, T.-H. (2012) Crystal Structure of the *Klebsiella pneumoniae* NFeoB/FeoC Complex and Roles of FeoC in Regulation of Fe2+ Transport by the Bacterial Feo System, *J. Bacteriol. 194,* 6518-6526.

[67] Stevenson, B., Wyckoff, E. E., and Payne, S. M. (2016) *Vibrio cholerae* FeoA, FeoB, and FeoC interact to form a complex, *J. Bacteriol. 198,* 1160-1170.

[68] Kim, H., Lee, H., and Shin, D. (2013) The FeoC Protein Leads to High Cellular Levels of the Fe(II) Transporter FeoB by Preventing FtsH Protease Regulation of FeoB in *Salmonella enterica*, *J. Bacteriol. 195,* 3364-3370.

[69] Kim, H., Lee, H., and Shin, D. (2015) Lon-mediated proteolysis of the FeoC protein prevents *Salmonella enterica* from accumulating the Fe(II) transporter FeoB under high-oxygen conditions, *J. Bacteriol. 197*, 92-98.

Table 1. Fits obtained for the Fe K-EXAFS of the as-isolated MBP-*Ec*FeoC, cleaved anaerobically reconstituted *Ec*FeoC, and cleaved anaerobically reconstituted *Kp*FeoC by curve fitting using the program EXCURVE 9.2.

		Fe-S			Fe-Fe			Fe-Fe			E_o[e]
Sample/fit	**Fit index[a]**	**No[b]**	**R[c] (nm) [Å]**	**DW[d] (nm^2) [$Å^2$]**	**No**	**R (nm) [Å]**	**DW (nm^2) [$Å^2$]**	**No**	**R (nm) [Å]**	**DW (nm^2) [$Å^2$]**	
MBP-*Ec*FeoC	0.75	3	0.226 [2.26]	0.00011 [0.011]	1	0.272 [2.72]	0.00005 [0.005]				0.743
Cleaved reconstituted *Ec*FeoC	0.49	4	0.226 [2.26]	0.00012 [0.012]	2	0.271 [2.71]	0.00005 [0.005]	1	0.2451 [2.541]	0.00004 [0.004]	2.256
Cleaved reconstituted *Kp*FeoC	0.92	4	0.231 [2.31]	0.00010 [0.010]	2	0.272 [2.72]	0.00006 [0.006]	1	0.2854 [2.854]	0.00007 [0.007]	-4.772

[a]The least-squares fitting parameter (see *Materials and Methods*) [b]Coordination number [c]Bond length [d]Debye-Waller factor [e]Photoelectron energy threshold

Figure Legends

Figure 1. The Feo system and the structure of *E. coli* FeoC. **A**. The arrangement of the *feo* operon in *E. coli* K-12, which encodes for three proteins: FeoA, FeoB, FeoC. FeoAp represents the location of the FeoA promoter. To emphasize the co-transcription of the components of the *feo* operon, the physical layout of neighboring genes such as a putative RNA-binding protein (encoded by *yhgF*) and a downstream nuclease (encoded by *rpnA*) is included. **B**. Cartoon of the Feo system in *E. coli*. FeoA (red) and FeoC (green) are small cytosolic proteins that may function as regulatory accessories to control ferrous (Fe^{2+}) iron transport. Movement of ferrous iron across a cellular membrane is accomplished by the large, polytopic membrane protein FeoB (purple). Hydrolysis of GTP to GDP within the N-terminal soluble GTP-binding domain of FeoB (NFeoB, teal) is thought to regulate opening and closing of FeoB, but it is unknown whether this process is driven in an active or facilitated manner. **C**. Lowest-energy NMR conformer of *Ec*FeoC (PDB ID 1XN7). Labeled regions are: the helix-turn-helix (HTH) motif and the unstructured wing region that contains four Cys residues (Cys^{56}, Cys^{61}, Cys^{64} and Cys^{70}) involved in [Fe-S] cluster binding. The labels "N" and "C" represent the amino and carboxy termini, respectively.

Figure 2. Construct design and purification of *Ec*FeoC. **A**. Because of poor native expression, *Ec*FeoC was expressed as a maltose-binding protein (MBP; salmon) fusion (MBP-*Ec*FeoC). On the N-terminus is encoded an additional $(His)_6$ tag (purple) for orthogonal purification. Preceding the *Ec*FeoC portion of the polypeptide (green) is an encoded TEV protease cleavage site. **B**. Cleaved, purified *Ec*FeoC is monomeric (≈ 9000 g/mol, 9 kDa) based on its gel-filtration retention volume on Superdex 75. The compared standards (K_{av} versus log MW, linearity R^2=0.97) are: blue dextran (void), alcohol dehydrogenase (150000 g/mol, 150 kDa), bovine serum albumin (66000

g/mol, 66 kDa), carbonic anhydrase (29000 g/mol, 29 kDa), cytochrome *c* (12000 g/mol, 12 kDa), and aprotinin (6500 g/mol, 6.5 kDa). **C**. SDS-PAGE analysis (acrylamide mass fraction of 15 %, left panel) and Tris-tricine gel analysis (gradient of acrylamide mass fraction from 10 % to 20 %, right panel), demonstrating *Ec*FeoC purity after cleavage and SEC. Black arrows indicate the location of the purified *Ec*FeoC. A small amount of dimeric *Ec*FeoC (≈ 18000 g/mol, 18 kDa) is observed in the Tris-tricine analysis at high protein concentration, but this dimeric species is only observed after freeze-thawing of the protein and cannot be dissociated by sample boiling.

Figure 3. **Figure 3**. Electronic absorption spectroscopy of *Ec*FeoC species suggests the presence of [Fe-S] clusters. **A**. Absorption spectrum of the MBP-*Ec*FeoC fusion protein aerobically as-isolated. **B**. Absorption spectrum of the cleaved apo *Ec*FeoC protein. **C**. Absorption spectrum of the cleaved, anaerobically reconstituted *Ec*FeoC protein. Solutions were kept at room temperature in a UV-transparent cuvette, and protein concentrations were generally 1 μmol/L to 20 μmol/L. Sample **A** was in MBP elution buffer, sample **B** was in TEV cleavage buffer, and sample **C** was in anaerobic reconstitution buffer (see Materials and Methods). Absorption data are normalized to the most intense band corresponding to the protein absorbance (280 nm), and each inset displays the full spectrum of each sample.

Figure 4. X-ray absorption spectroscopy (XAS) indicates the presence of [Fe-S] clusters in *Ec*FeoC. Fe K-edge X-ray absorption fine structure (EXAFS) and Fourier transforms of MBP-*Ec*FeoC (**A**) and anaerobically reconstituted *Ec*FeoC (**B**). For ease of interpretation, data are graphed as Fourier transform amplitude versus distance (R) in Å, where 1 Å = 0.1 nm. Black traces represent the experimental data, and red traces represent the simulations. Parameters used to

generate the simulated spectra are listed in Table 1. Sample **A** was in 25 mmol/L Tris buffer, pH 7.5, 200 mmol/L NaCl, 10 mmol/L maltose, 3.6 mol/L ethylene glycol (20% (v/v)), and 0.7 mol/L glycerol (5% (v/v)). Sample **B** was in 50 mmol/L MOPS buffer, pH 7.5, 150 mmol/L NaCl, 10 mmol/L DTT, and 3.6 mol/L ethylene glycol (20% (v/v)).

Figure 5. Electron paramagnetic resonance (EPR) spectroscopy indicates the identity of the observed [Fe-S] clusters in *Ec*FeoC. Continuous-wave (CW) X-band EPR spectra of MBP-*Ec*FeoC as-isolated (**A**), MBP-*Ec*FeoC reduced with sodium dithionite (**B**), cleaved and anaerobically-reconstituted *Ec*FeoC (**C**), and cleaved and anaerobically-reconstituted *Ec*FeoC reduced with sodium dithionite (**D**). Samples **A** and **B** were in 25 mmol/L Tris buffer, pH 7.5, 200 mmol/L NaCl, 10 mmol/L maltose, 3.6 mol/L ethylene glycol (20% (v/v) ethylene glycol), and 0.7 mol/L glycerol (5% (v/v) glycerol) ± 1 mmol/L sodium dithionite, respectively. Samples **C** and **D** were in 50 mmol/L MOPS buffer, pH 7.5, 150 mmol/L NaCl, 10 mmol/L DTT, and 3.6 mol/L ethylene glycol (20% (v/v) ethylene glycol) ± 1 mmol/L sodium dithionite, respectively. Samples **A** and **C** are plotted on identical scales, and samples **B** and **D** are plotted on identical scales. Spectral parameters were as follows: (**A**) 20 K, modulation amplitude = 0.5 mT, modulation frequency = 100 kHz, 1024 points, conversion time = 117.19 ms, microwave power = 9.5 mW, 4 scans (**B**) 20 K, modulation amplitude = 0.5 mT, modulation frequency = 100 kHz, 1024 points, conversion time = 87.89 ms, microwave power = 9.5 mW, 16 scans (**C**) 6 K, modulation amplitude = 0.5 mT, modulation frequency = 100 kHz, 1024 points; conversion time = 117.19 ms, microwave power = 4.7 mW, 1 scan (**D**) 6 K, modulation amplitude 0.5 mT, modulation frequency = 100 kHz, 1024 points, conversion time = 87.89 ms, microwave power = 1.9 mW, 16 scans. A cavity

contaminant marked by an asterisk (*) at ≈ 335 mT (g ≈ 2.005) was observed even after background subtraction in all spectra.

Figure 6. The $[4Fe\text{-}4S]^{2+}$ cluster of *Ec*FeoC is rapidly oxygen sensitive. **A**. Representative time course spectra of cleaved, anaerobically reconstituted *Ec*FeoC reacting with air-saturated buffer. Spectra were taken every 6 s (black, dotted) immediately after buffer mixing until reactivity stopped (≈ 5 min). The $[4Fe\text{-}4S]^{2+}$ spectral features (goldenrod) are rapidly lost and the appearance of the $[2Fe\text{-}2S]^{2+}$ spectral features rapidly appear (purple). The inset represents the plots of the two species before (goldenrod) and after (purple) reaction. The sample was in 50 mmol/L MOPS buffer, pH 7.5, 150 mmol/L NaCl, and 1 mmol/L TCEP at room temperature. **B**. Representative plot of the kinetic decay of the absorbance feature at 400 nm (closed circles), characteristic of the $[4Fe\text{-}4S]^{2+}$ cluster, and its fitted simulation (black dashed line), revealing a k_{obs} of (0.037 ± 0.010) s^{-1} and a $t_{½}$ of (19 ± 4.8) s when averaged over three replicates.

Figure 7. *Kp*FeoC also binds an redox-active, oxygen-sensitive [4Fe-4S] cluster. **A**. Absorption spectrum of the cleaved, anaerobically reconstituted *Kp*FeoC protein. Conditions were the same is in Figure 3C. **B**. Fe EXAFS and Fourier transforms of anaerobically reconstituted *Kp*FeoC. Conditions were the same as in Figure 4B. **C**. CW X-band EPR spectrum of cleaved and anaerobically-reconstituted *Kp*FeoC reduced with sodium dithionite. Sample conditions were the same as in Figure 5D. Data collection parameters were as follows: 10 K, modulation amplitude 0.5 mT, modulation frequency = 100 kHz, 1024 points, conversion time = 58.59 ms, microwave power = 0.47 mW, 16 scans. A cavity contaminant marked by an asterisk (*) at ≈ 335 mT (g ≈ 2.005) was observed even after background subtraction in all spectra. **D**. Representative time

course spectra of cleaved, anaerobically reconstituted *Kp*FeoC reacting with air-saturated buffer. Spectra were taken every 6 s (black, dotted) immediately after buffer mixing until reactivity stopped. The $[4Fe\text{-}4S]^{2+}$ spectral features (goldenrod) are rapidly lost and the appearance of the $[2Fe\text{-}2S]^{2+}$ spectral features rapidly appear (purple). The inset represents the plot of the kinetic decay of the absorbance feature at 400 nm (closed circles), characteristic of the $[4Fe\text{-}4S]^{2+}$ cluster, and its fitted simulation (black dashed line), revealing a k_{obs} of (0.030 ± 0.020) s^{-1} and a $t_{½}$ of (34 ± 15) s when averaged over three replicates

Figure 8. *Ec*FeoC does not dimerize in the presence of the $[4Fe\text{-}4S]^{2+}$ cluster. Representative dynamic light scattering (DLS) data of apo (dashed) and $[4Fe\text{-}4S]^{2+}$-bound forms (solid) of *Ec*FeoC plotted as number (**A**), volume (**B**), or intensity (**C**) versus globular diameter, clearly demonstrating the cluster-bound form assumes a more compact shape than the apo form of *Ec*FeoC. Samples were in 50 mmol/L MOPS buffer, pH 7.5, 150 mmol/L NaCl, and 1 mmol/L DTT at room temperature.

Figure 9. The observed forms of the redox-active, oxygen-sensitive cluster in *Ec*FeoC. Under strictly anaerobic conditions (such as those that may be operative within *E. coli* during anaerobic growth), a $[4Fe\text{-}4S]^{2+/+}$ cluster is observed. Upon reaction with oxygen-replete buffer, the $[4Fe\text{-}4S]^{2+}$ rapidly decays to a $[2Fe\text{-}2S]^{2+}$ cluster. After prolonged exposure to oxygen, a rubredoxin-like decay product (*i.e.*, $[Fe^{3+}(Cys)_4]$) is observed. Unlike FNR, we have yet to observe a $[3Fe\text{-}4S]^{+/0}$ cluster bound to *Ec*FeoC (indicated by the presence of brackets), but we surmise the transformation from $[4Fe\text{-}4S]^{2+}$ to $[2Fe\text{-}2S]^{2+}$ contains this transient species. This oxygen-

responsive cluster disassembly may represent the behavior *Ec*FeoC undergoes *in vivo* during the organism's transition from anaerobic growth to aerobic growth.

Figure 1.

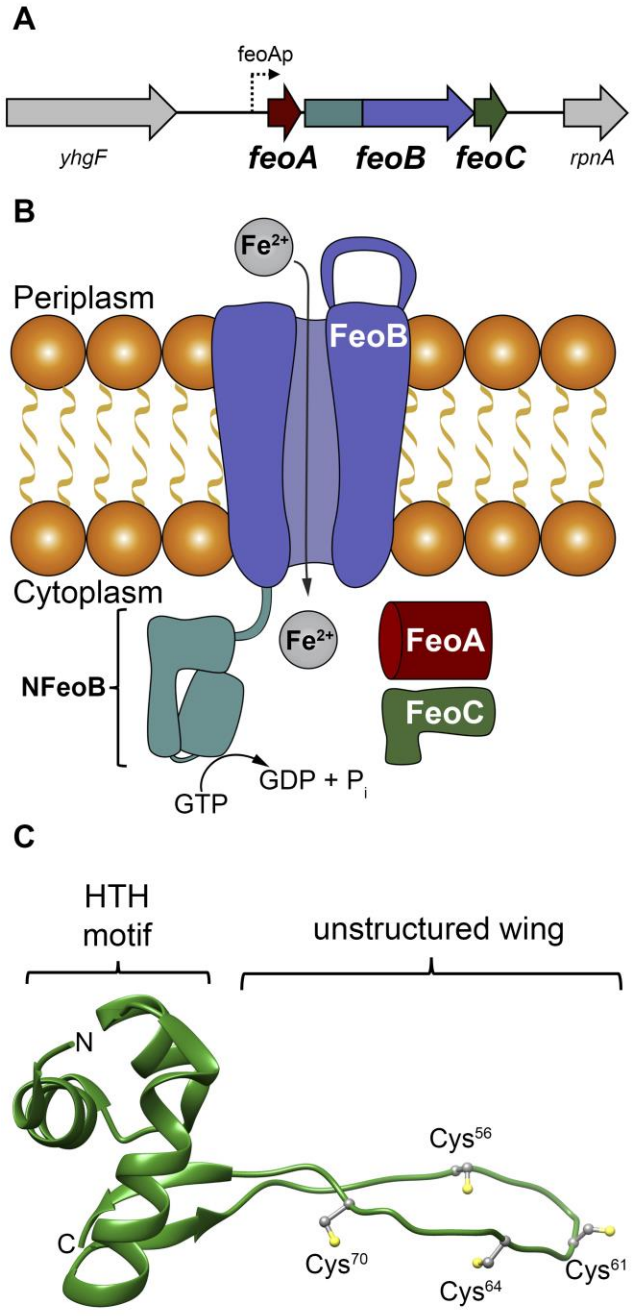
A
feoAp
yhgF
feoA
feoB
feoC
rpnA
B
Fe2+
Periplasm
FeoB
Cytoplasm
Fe2+
FeoA
NFeoB
FeoC
GTP
GDP + Pi
C
HTH
motif
unstructured wing
N
C
Cys56
Cys70
Cys64
Cys61

Figure 2.

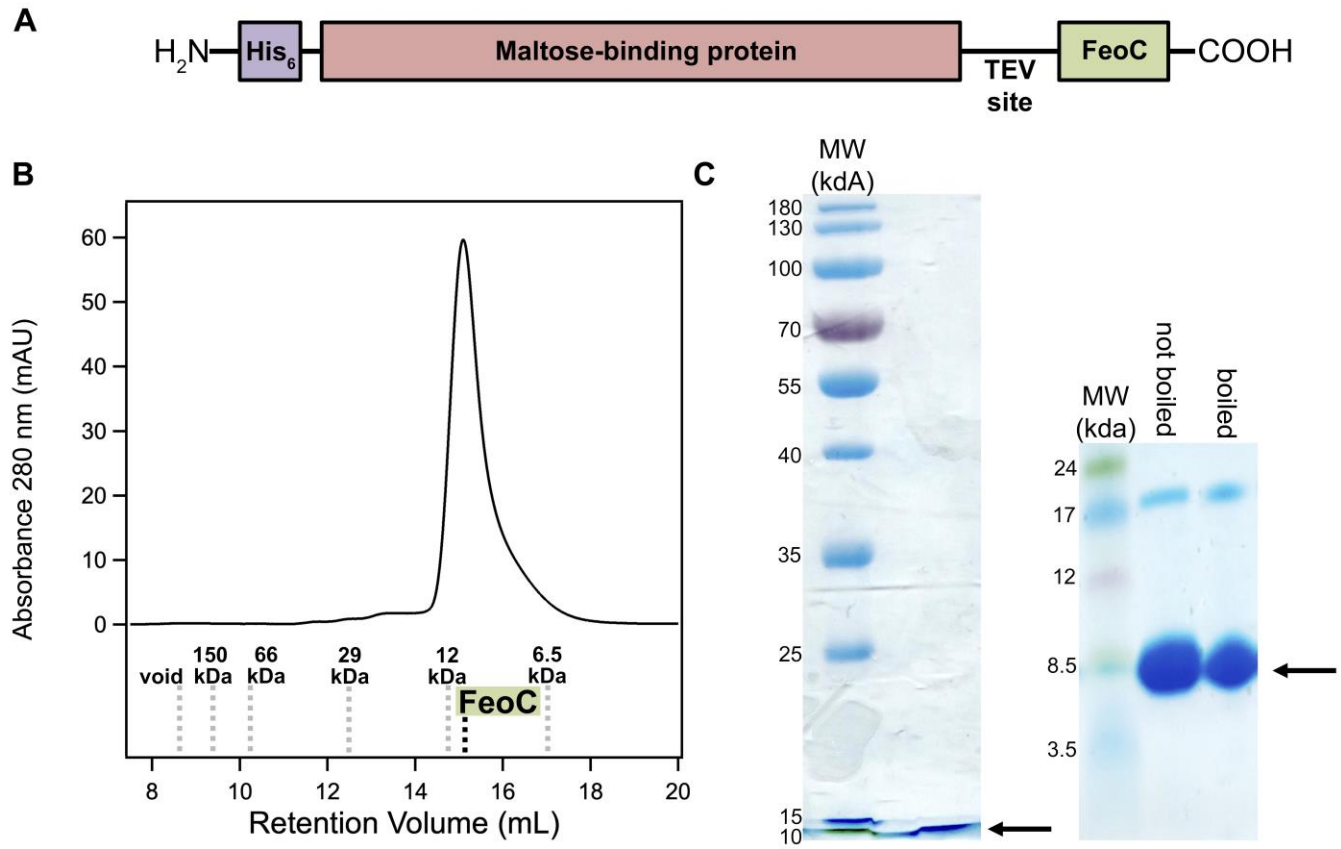
A
H2N
His6
Maltose-binding protein
TEV site
FeoC
COOH
B
Absorbance 280 nm (mAU)
Retention Volume (mL)
void
150 kDa
66 kDa
29 kDa
12 kDa
6.5 kDa
FeoC
C
MW (kdA)
180
130
100
70
55
40
35
25
15
10
MW (kda)
not boiled
boiled
24
17
12
8.5
3.5

Figure 3.

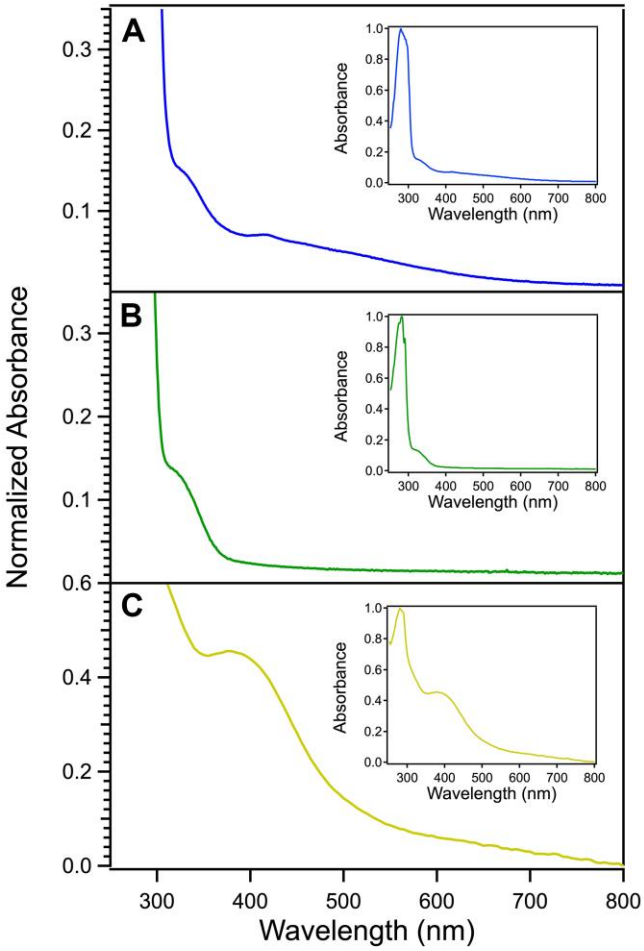
A
B
C
Normalized Absorbance
Wavelength (nm)
Absorbance
Wavelength (nm)

Figure 4.

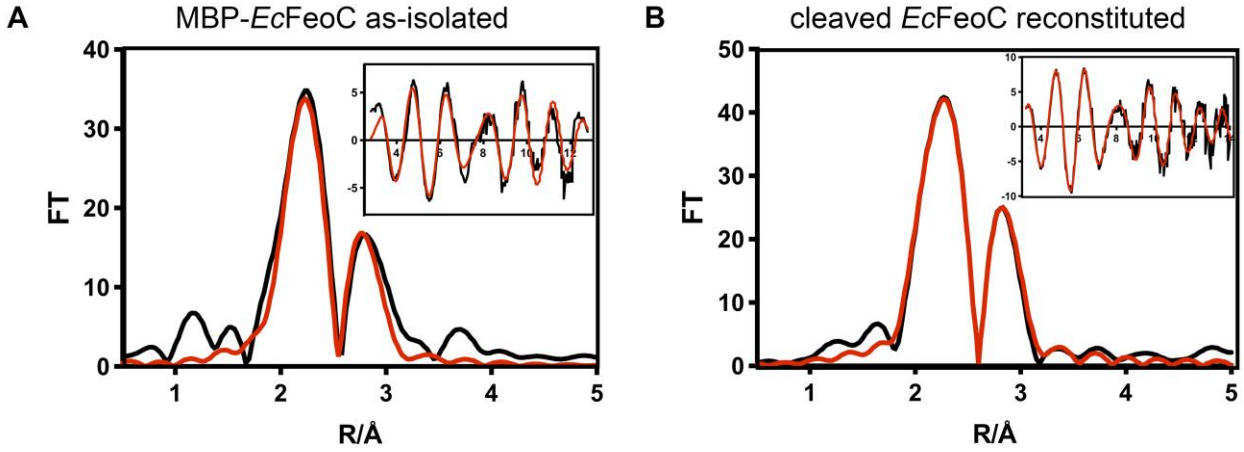
A
MBP-*Ec*FeoC as-isolated
FT
R/Å
B
cleaved *Ec*FeoC reconstituted
FT
R/Å

Figure 5.

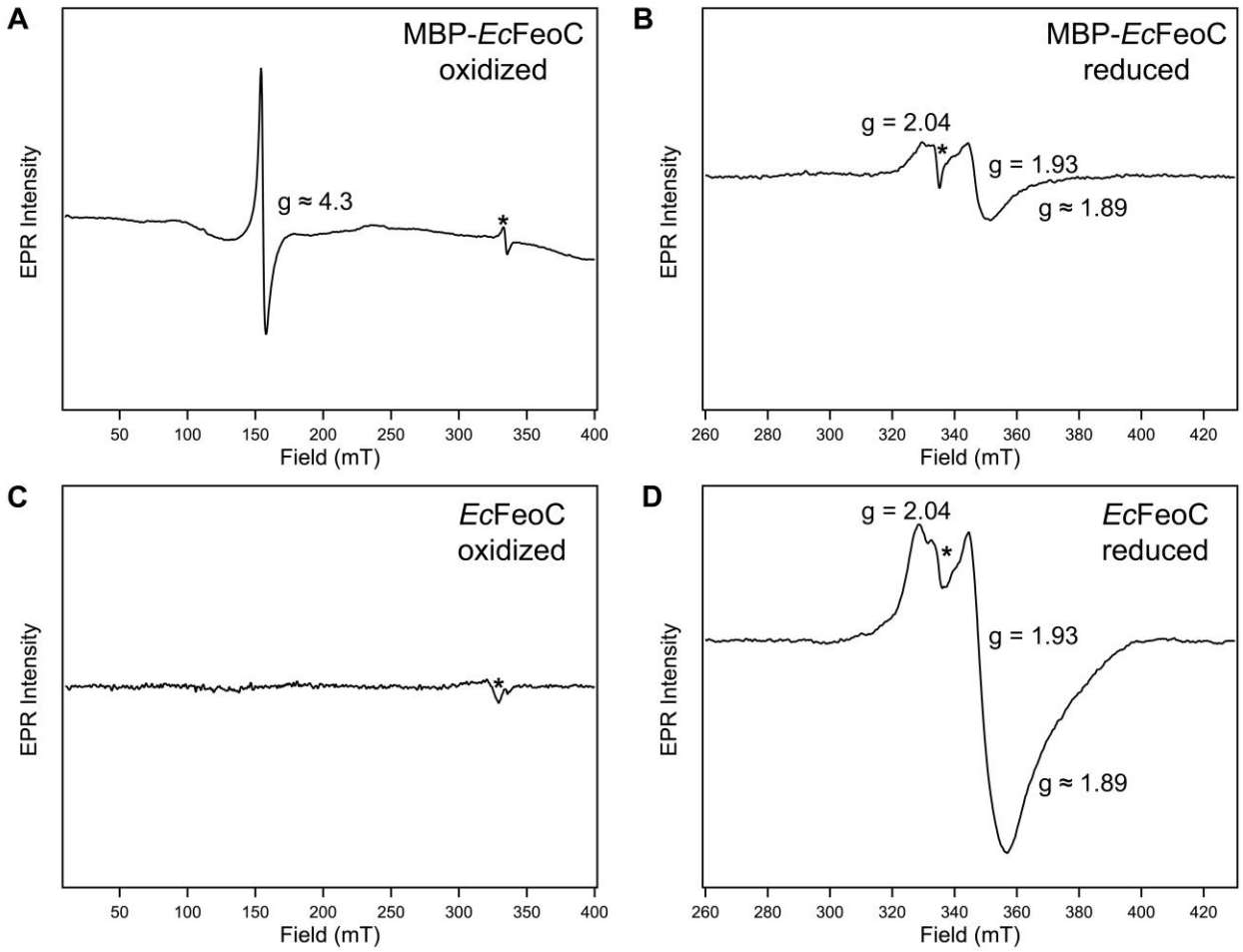
A
MBP-*Ec*FeoC
oxidized
g ≈ 4.3
*
EPR Intensity
50 100 150 200 250 300 350 400
Field (mT)
B
MBP-*Ec*FeoC
reduced
g = 2.04
*
g = 1.93
g ≈ 1.89
EPR Intensity
260 280 300 320 340 360 380 400 420
Field (mT)
C
*Ec*FeoC
oxidized
*
EPR Intensity
50 100 150 200 250 300 350 400
Field (mT)
D
g = 2.04
*
*Ec*FeoC
reduced
g = 1.93
g ≈ 1.89
EPR Intensity
260 280 300 320 340 360 380 400 420
Field (mT)

Figure 6.

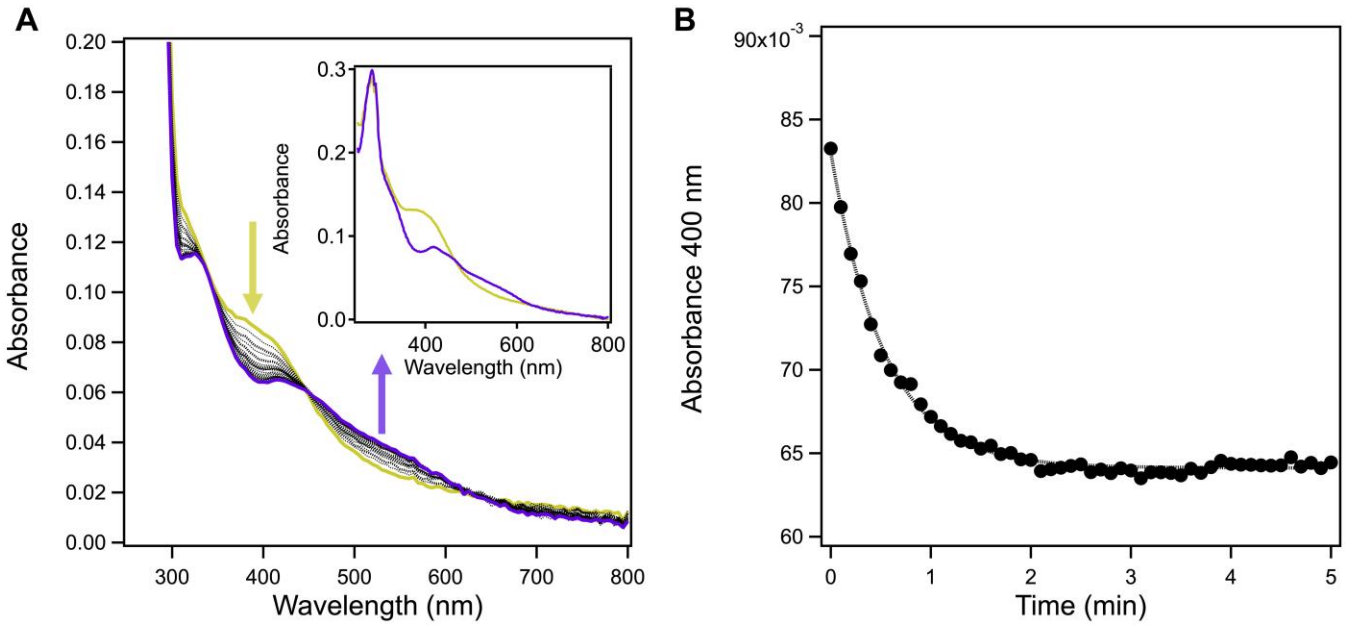
A
Absorbance
Wavelength (nm)
Absorbance
Wavelength (nm)
B
90x10-3
Absorbance 400 nm
Time (min)

Figure 7.

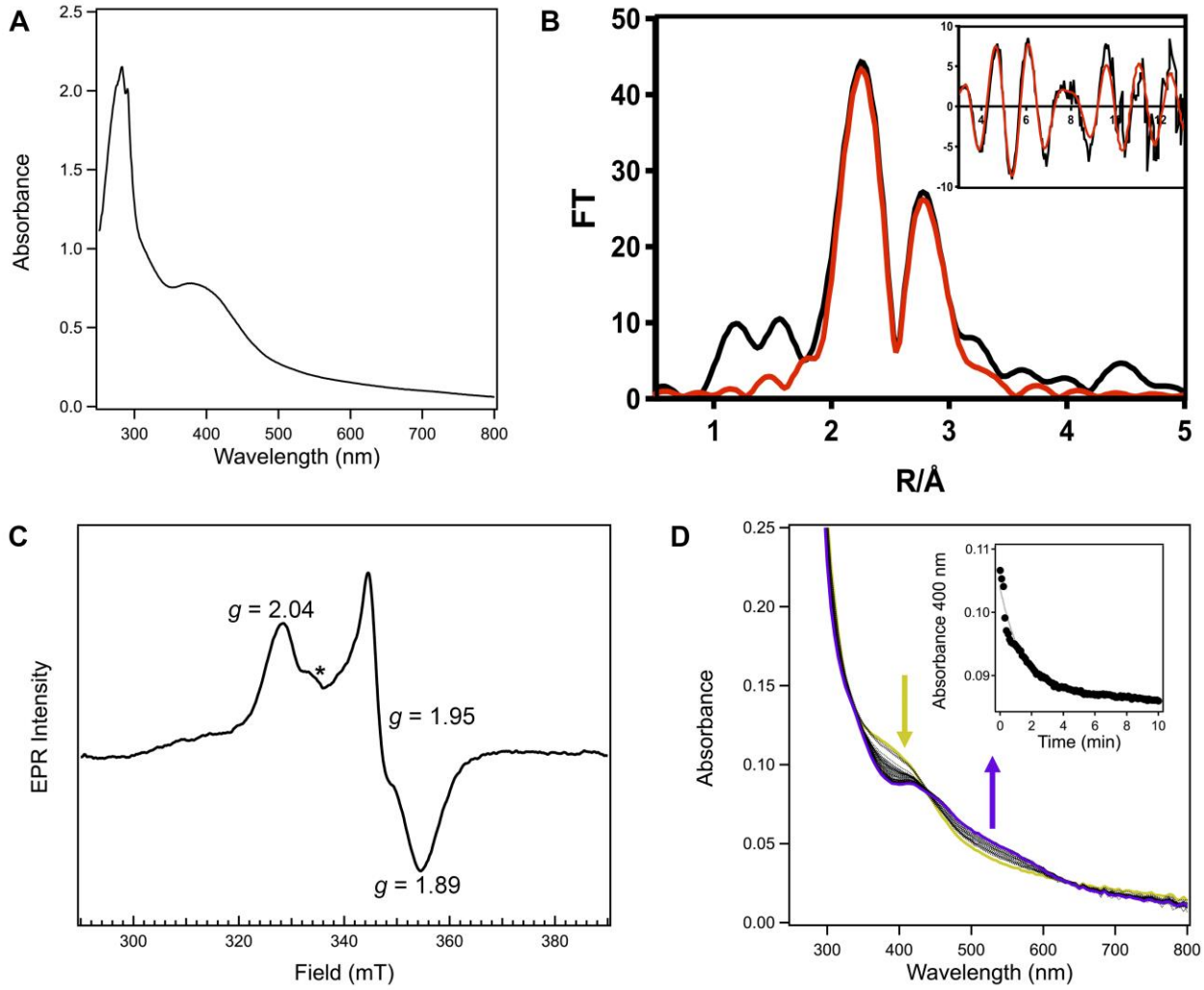
A
Absorbance
Wavelength (nm)
B
FT
R/Å
C
EPR Intensity
g = 2.04
g = 1.95
g = 1.89
Field (mT)
D
Absorbance
Absorbance 400 nm
Time (min)
Wavelength (nm)

Figure 8.

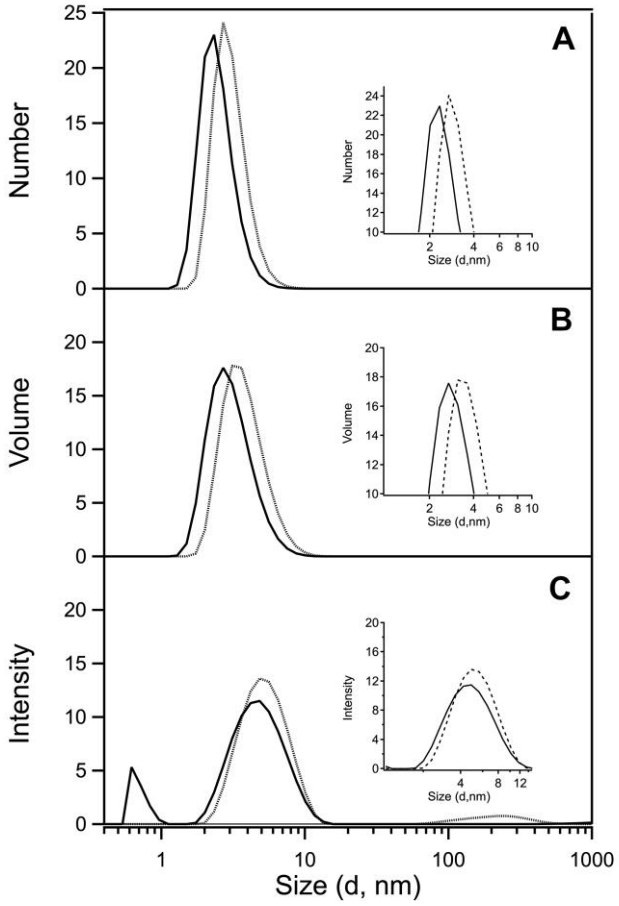

Figure 9.

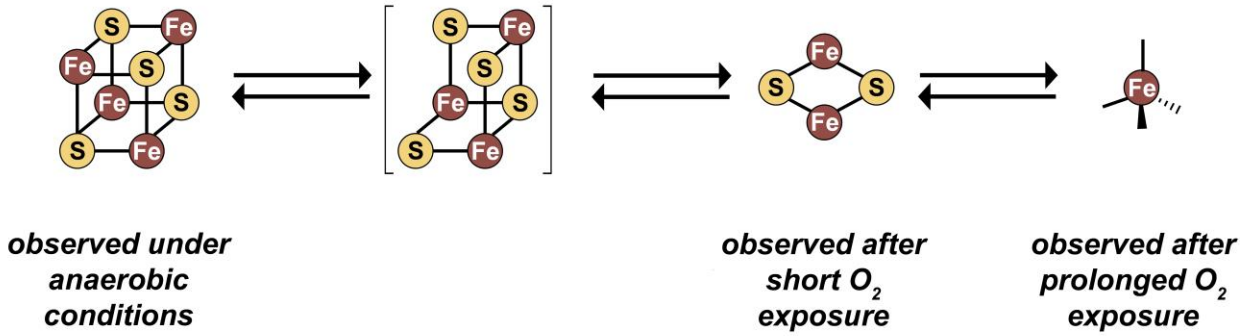
S
Fe
observed under anaerobic conditions
observed after short O_2 exposure
observed after prolonged O_2 exposure

SUPPORTING INFORMATION

Figure S1. The purification and cleavage of the MBP-*Ec*FeoC fusion. **A**. SDS-PAGE analysis (acrylamide mass fraction of 15 %) of the intact and cleaved forms of MBP-*Ec*FeoC. MW: molecular weight marker lane; lane 1: purified MBP-*Ec*FeoC fusion; lane 2: cleavage mixture of MBP-*Ec*FeoC after treatment with TEV protease; lanes 3-5: Superdex 75 SEC fractions; lane 6: empty; lane 7: final purified, concentrated cleaved *Ec*FeoC. **B**. Superdex 75 size-exclusion chromatogram of the cleavage mixture in panel **A**, lane 2. V: void volume; 3: panel **A**, lane 3 (protein aggregate); 4: panel **A**, lane 4 ($(His)_6$-MBP); 5: panel **A**, lane 5 (cleaved *Ec*FeoC prior to concentrating).

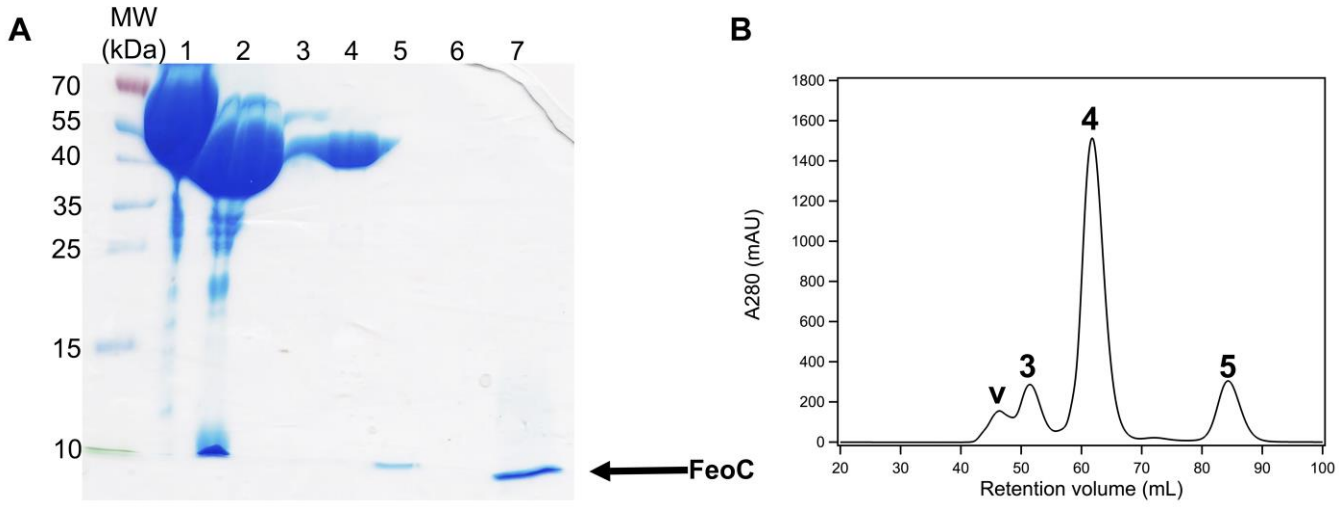

Figure S2. Far-UV circular dichroism spectrum of cleaved, apo *Ec*FeoC. Protein (0.1 mg/mL) was contained within in a UV-transparent quartz cuvette in phosphate-buffered saline (PBS; 0.137 mol/L NaCl, 0.0027 mol/L KCl, 0.01 mol/L Na_2HPO_4, 0.0018 mol/L KH_2PO_4, pH 7.4) at room temperature. The shown spectrum represents the average of 5 spectra.

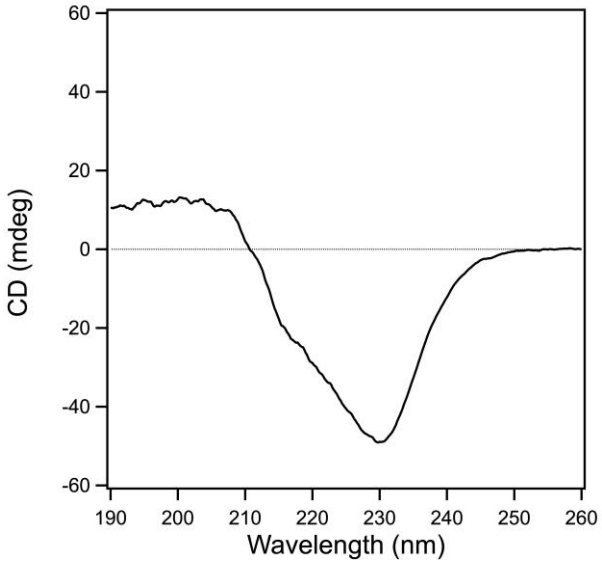

Figure S3. Electronic absorption spectra of as-isolated MBP-*Ec*FeoC prior (blue spectrum) and after (black spectrum) the addition of sodium dithionite. Samples were at room temperature in 25 mmol/L Tris buffer, pH 7.5, 200 mmol/L NaCl, 10 mmol/L maltose, and 0.7 mol/L glycerol (5 % (v/v) without (blue) or with (black) 1 mmol/L sodium dithionite.

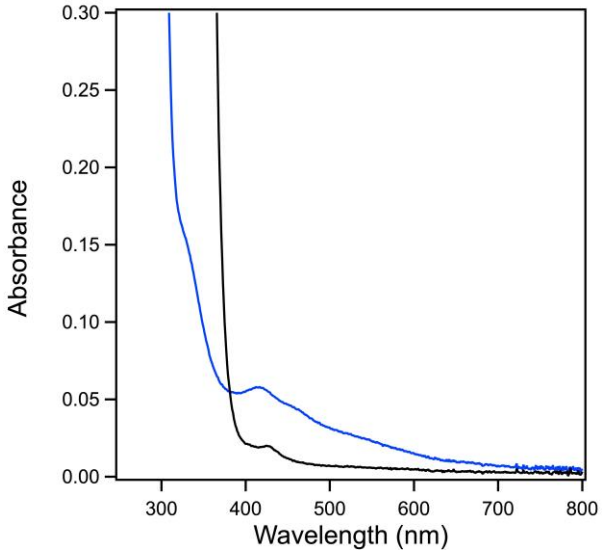

Figure S4. Room temperature electronic absorption spectrum of $[4Fe\text{-}4S]^{2+}$-bound to cleaved, anaerobically-reconstituted *Ec*FeoC. Molar absorptivity values are calculated as $mM^{-1}cm^{-1}$ per molar equivalent iron.

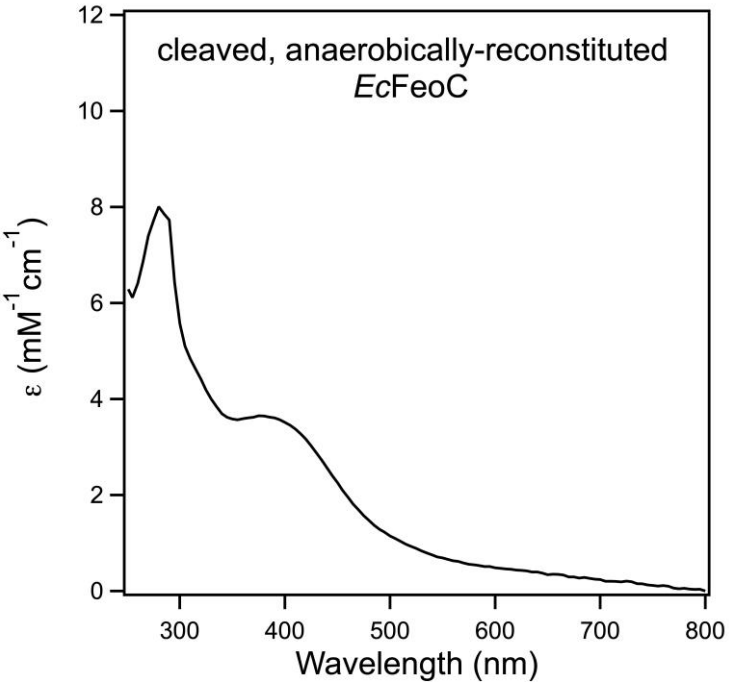

Figure S5. The $[4Fe\text{-}4S]^{2+}$ cluster of *Ec*FeoC is rapidly oxygen sensitive. **A**. Representative time course spectra of cleaved, anaerobically reconstituted *Ec*FeoC reacting upon the exposure to ambient atmosphere. Spectra were taken every 6 s (for clarity, only spectra every 30 s are displayed black and dotted) immediately after exposure of the previously anaerobic sample to air until reactivity stopped (≈ 15 min). The $[4Fe\text{-}4S]^{2+}$ spectral features (goldenrod) are rapidly lost and the appearance of the $[2Fe\text{-}2S]^{2+}$ spectral features rapidly appear (purple). The inset represents the plots of the two species before (goldenrod) and after (purple) reaction. The sample was in 50 mmol/L MOPS buffer, pH 7.5, 150 mmol/L NaCl, and 1 mmol/L TCEP at room temperature. **B**. Representative plot of the kinetic decay of the absorbance feature at 400 nm (closed circles), characteristic of the $[4Fe\text{-}4S]^{2+}$ cluster. The presence of a lag phase (≈ 0 min to 6 min) and two separate kinetic phases (≈ 6min to 10 min and ≈ 10 to 14 min) are seen, but these may be due to the limited diffusion of O_2 into degassed buffer.

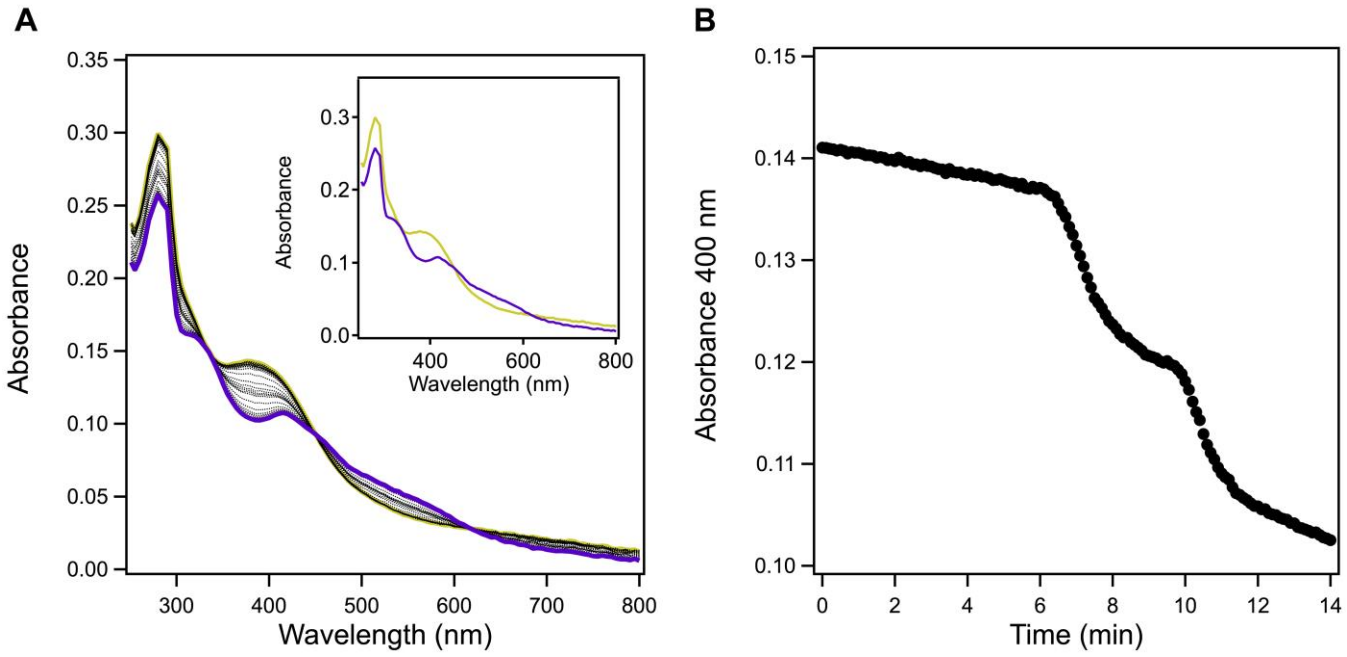

Figure S6. The purification and cleavage of the MBP-*Kp*FeoC fusion. Tris-tricine gel analysis (gradient of acrylamide mass fraction from 10 % to 20 %, right panel), demonstrating *Kp*FeoC purity after cleavage and SEC. MW: molecular weight marker lane; lane 1: purified MBP-*Kp*FeoC fusion; lane 2: cleavage mixture of MBP-*Kp*FeoC after treatment with TEV protease; lane 3: monomeric, cleaved *Kp*FeoC after SEC on Superdex 75; lane 4: final concentrated monomeric, cleaved *Kp*FeoC.

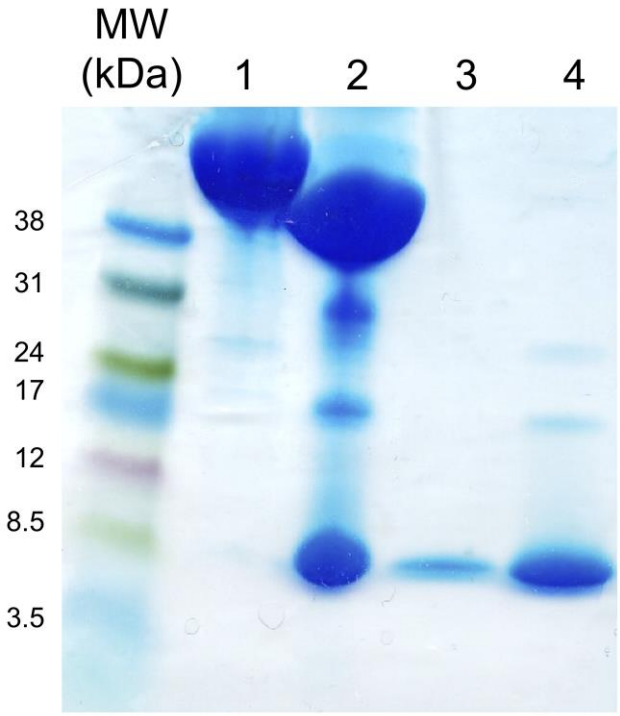

Figure S7. Electronic absorption spectra of as-isolated MBP-*Kp*FeoC prior to enzymatic cleavage. Sample conditions were the same as in Figure S3.

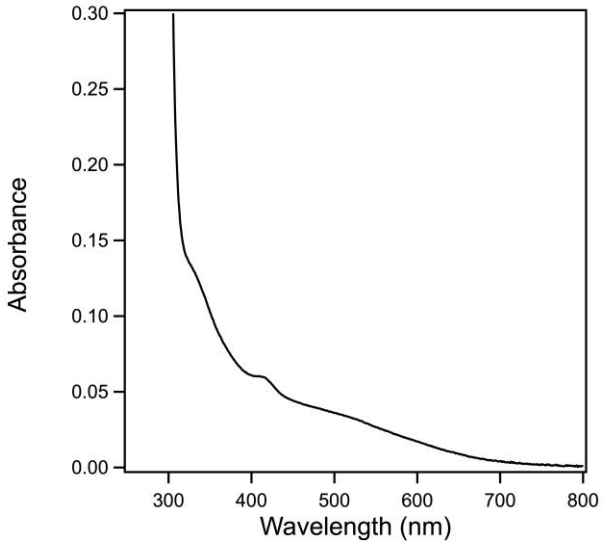

Figure S8. EPR spectroscopy indicates the identity of several of the observed [Fe-S] clusters in *Kp*FeoC. CW X-band EPR spectra of MBP-*Kp*FeoC as-isolated (**A**), MBP-*Kp*FeoC reduced with sodium dithionite (**B**), and cleaved and anaerobically-reconstituted *Kp*FeoC prior to reduction with sodium dithionite (**C**). Data collection parameters were similar to those in Figure 5. A cavity contaminant marked by an asterisk (*) at ≈ 335 mT (g ≈ 2.005) was observed even after background subtraction in all spectra.

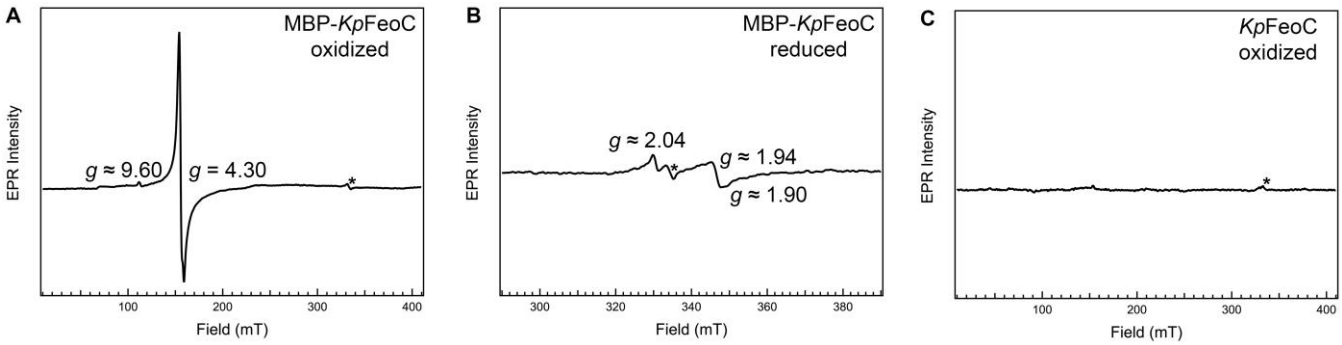

Figure S9. Room temperature electronic absorption spectrum of $[4Fe\text{-}4S]^{2+}$-bound to cleaved, anaerobically reconstituted *Kp*FeoC. Molar absorptivity values are calculated as $mM^{-1}cm^{-1}$ per molar equivalent iron.

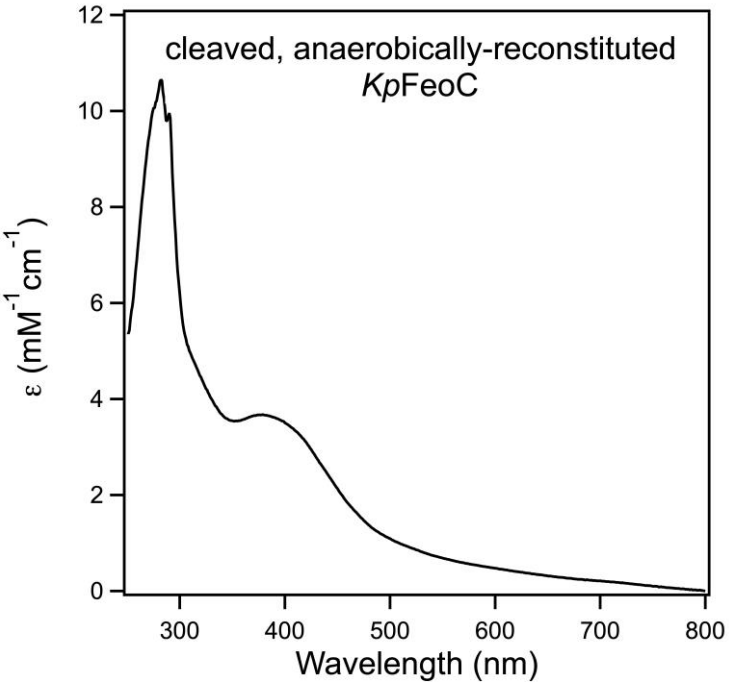

Figure S10. *Kp*FeoC also does not dimerize in the presence of the $[4Fe\text{-}4S]^{2+}$ cluster. Representative dynamic light scattering (DLS) data of apo (gray dashed) and $[4Fe\text{-}4S]^{2+}$-bound forms (solid) of *Kp*FeoC plotted as number (top panel), volume (middle panel), or intensity (bottom panel) versus globular diameter.

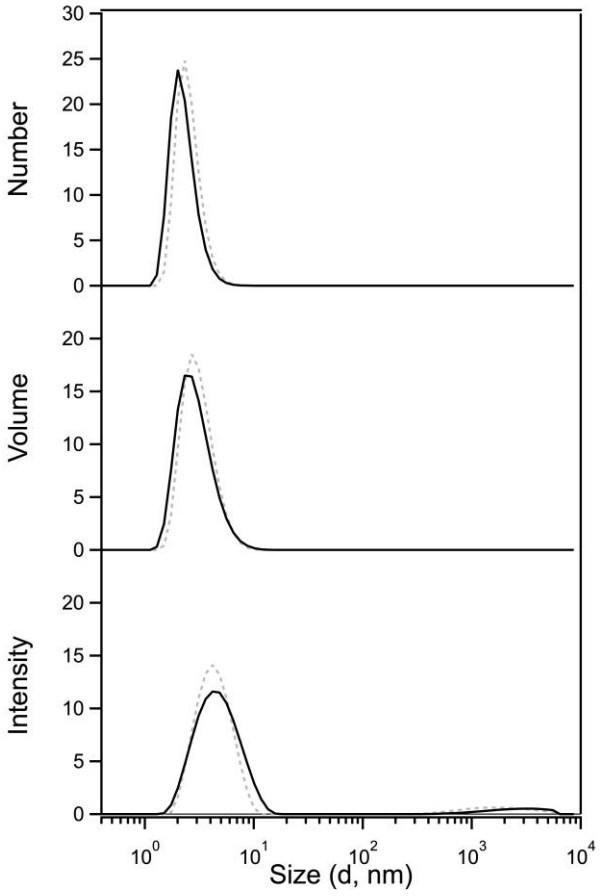

Figure S11. After oxidation of the $[4Fe\text{-}4S]^{2+}$ cluster to the $[2Fe\text{-}2S]^{2+}$ cluster and filtration, *Ec*FeoC remains monomeric (≈ 9000 g/mol, 9 kDa) based on its gel-filtration retention volume on Superdex 75.